INTERNATIONAL ATOMIC ENERGY AGENCY
UNITED NATIONS EDUCATIONAL, SCIENTIFIC AND CULTURAL ORGANIZATION

INTERNATIONAL CENTRE FOR THEORETICAL PHYSICS
34100 TRIESTE (ITALY) - P.O.B. 586 - MIRAMARE - STRADA COSTIERA 11 - TELEPHONES: 224281/2/3/4/5/6
CABLE: CENTRATOM - TELEX 460392-I

SMR/115 - 57

WINTER COLLEGE ON LASERS, ATOMIC AND MOLECULAR PHYSICS

(21 January - 22 March 1985)

LASER TECHNIQUES IN CHEMICAL DIAGNOSTICS

J.P. TARAN
Office National d'Etudes et des Recherches Aérospatiales
92320 Chatillon
France

FR ISSN 0078-3781

ONERA

OFFICE NATIONAL D'ÉTUDES ET DE RECHERCHES AÉROSPATIALES

LASER TECHNIQUES IN CHEMICAL DIAGNOSTICS

by

Brigitte ATTAL

NOTE TECHNIQUE 1981-8

LASER TECHNIQUES IN CHEMICAL DIAGNOSTICS

by

Brigitte ATTAL

Stagiaire de thèse à l'ONERA

OFFICE NATIONAL D'ÉTUDES ET DE RECHERCHES AÉROSPATIALES

29, Avenue de la Division Leclerc, 92320 CHATILLON (France)

TABLE

LASER TECHNIQUES IN CHEMICAL DIAGNOSTICS

by Brigitte ATTAL

SUMMARY

Optical diagnostics techniques which are applicable to fluid dynamics, combustion research and atmospheric sounding, have been used for many years.

The introduction of the laser gave great impetus to the development of these techniques which can provide informations like temperature or concentration, non intrusively accurately and if possible remotely.

We will discuss only three of these laser techniques in this course, namely : laser-induced fluorescence (LIF), spontaneous Raman scattering (SRS) and coherent anti-stokes Raman scattering (CARS). They are currently the most widely used for the diagnostics of flowfields and combustions.

Keywords (NASA thesaurus) : Optical measurement · Laser applications · Raman Spectroscopy · Raman scattering · Fluorescence · Flow characteristics · Combustion temperature.

♦

LES METHODES OPTIQUES EN CHIMIE ANALYTIQUE

RÉSUMÉ

Les méthodes optiques sont de plus en plus utilisées comme méthodes d'investigation dans les flammes et les écoulements aérodynamiques ou pour l'étude de l'atmosphère.

Actuellement, l'utilisation du laser est à l'origine du développement important de ces méthodes ; elles peuvent fournir des informations telles que température et concentrations, avec précision et sans qu'aucune sonde ne perturbe l'échantillon.

Nous limiterons la discussion aux trois techniques les plus couramment utilisées pour l'analyse de combustion et d'écoulements : la fluorescence, la diffusion Raman spontanée et la diffusion Raman anti-stokes cohérente.

Mots clés (lexique CEDOCAR) : Exploration optique · Température combustion · Diffusion Raman · Diffusion Raman AntiStokes Cohérente · Fluorescence · Spectroscopie laser · Ecoulement fluide.

INTRODUCTION

The search for new and improved diagnostic techniques applicable to fluid dynamics, combustion research and atmospheric sounding has been actively pursued for many years in several laboratories. Specifically, the purpose has been the development and implementation of techniques which were to provide most of the necessary informations nonintrusively, accurately and if possible remotely. The techniques also were to be of adequate sensitivity (1 to 1000 ppm) and resolution capability (1 to 10 mm).

The desire to perform the measurements nonintrusively immediately suggests the use of optical diagnostic techniques. The introduction of the laser gave great impetus to the development of these techniques which are based essentially upon interaction of photons with particles. The processes of interest used for diagnostic purposes are specifically :

- Mie scattering [1], absorption [2], fluorescence [3-7], Rayleigh [8, 9], Raman [10-14], resonance Raman [15] which are all spontaneous scattering processes, coherent anti-Stokes Raman scattering known as CARS [16, 17] and related non linear optical processes such as RIKE and SRGS.

In order to compare the potential of spontaneous scattering phenomena, a common convenient parameter known as the scattering cross-section (in units cm^2/sr) can be introduced. The scattering cross-section associated with these processes vary over a large range and typically are of the order of 10^{-8} cm^2/sr for Mie scattering, 10^{-20} cm^2/sr for absorption and fluorescence, 10^{-27} cm^2/sr for Rayleigh, 10^{-30} cm^2/sr for Raman scattering. The resonance Raman scattering cross-section may be up to six orders of magnitude higher than the spontaneous vibrational Raman scattering. The nonlinear optical techniques on the other hand, are characterized by large signal strength good spatial resolution, but also present specific and delicate problems and are costly. The technique with the larger scattering cross-section seems a priori more attractive. However, cross-section is only one of the characteristic parameters and all the aspects of any particular technique have to be considered carefully in performing a particular measurement in a particular situation. We will discuss only some of these laser techniques, namely : fluorescence, spontaneous Raman scattering and CARS which are currently the most widely used for the diagnostics of flowfields and combustions.

The laser induced fluorescence technique or LIF is an attractive method for making density measurements without the use of flow disturbing probes [18]. Laser excitation has been used to determine the fluorescence spectral characteristics of a number of molecular species in various flames [19-24]. Tunable dye lasers are the most commonly used sources for this work [6, 25]. LIF will be discussed in the first chapter.

The possibility of carrying out time-averaged and time-resolved temperature and concentration measurements in flames as well as time-resolved measurements in turbulent flows by Raman spectroscopy is discussed in the second chapter. Detailed accounts of early experimental work can be found in several project SQUID and AIAA workshop proceedings[26-29]. Important instrumental developments were accomplished, such as the improvement in collection efficiencies and in signal to noise ratio. Many results on flames [30, 31] and aerodynamic flows [32, 33] have been reported. The first part of the presentation briefly reviews the main properties of spontaneous Raman scattering (SRS) and describes how temperature and number density are obtained from the spectral data. The measurement techniques are described and the problems encountered with pulsed lasers are discussed.

It appears that SRS can be valuable for the investigation of such easily analysed samples as cold or warm aerodynamic jets, but SRS is of limited potential in low pressure gases, fluorescent samples or in luminous reactive media. CARS, with much improved signal strength, provides an alternative to SRS in the specific area of combustion diagnostics and is presented in the third chapter. CARS, which was first observed in 1963 [34, 35], is but one of many well-known third-order processes. Raman spectroscopy by CARS received a considerable impetus in the early seventies when reliable tunable sources of good optical quality were developed. The theory of CARS is first reviewed and several results are then discussed.

In the last part of chapter III, we present a study of electronic resonance enhancement in CARS, which shows great promise for sensitive detection of trace species and for high resolution molecular spectroscopy.

I - LASER INDUCED FLUORESCENCE (L.I.F.)

1 - INTRODUCTION

When a beam of light passes through a gas, part of this light will interact with the molecules and be re-emitted in all directions. A fraction of this light can be collected and analysed to determine some of the properties of the gas, using an arrangement such as that shown schematically in Fig. 1. The fluorescence process is initiated by irradiating the molecules with a laser tuned to a particular electronic absorption line. The molecules are excited into the upper state of the transition. After some time delay, called the natural lifetime (typically 10^{-9} s), the molecules reemit light while undergoing a transition to the initial ground electronic state, provided that they are not first de-excited by some non-radiative process. The fluorescence energy-level diagram for a molecule which is excited by a monochromatic laser radiation is shown in Fig. 2.

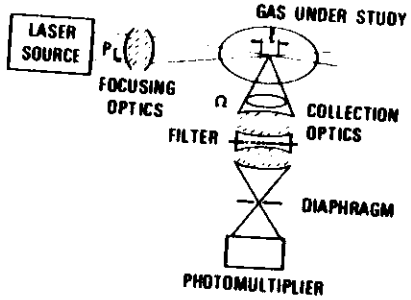

Fig. 1 - Typical experimental arrangement for LIF and SRS ; P_L is the intensity of the incident beam, ℓ the length along the incident beam from which the scattered light is collected and Ω is the solid angle of collection optics.

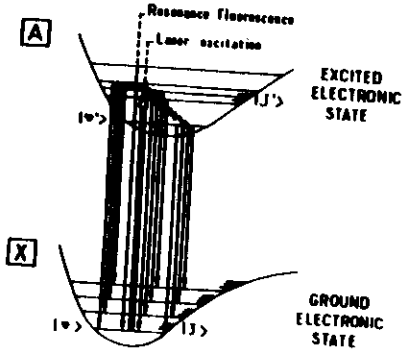

Fig. 2 - Energy transitions of laser induced fluorescence. During the natural lifetime of the excited rovibronic level, vibrational or rotational redistribution (wavy arrows) may occur in the excited state manifold as a result of collisions, prior to re-emission of light.

During the time the molecule remains in the excited electronic state (10^{-9} s), it is likely to undergo collisions with other molecules ; the collision rate at STP is on the order of 10^{10} per second. These collisions can have several effects. One effect is that they can cause the absorbing molecule to lose "memory" of the direction and polarization of the incident beam, increasing the depolarization and isotropy of the fluorescence. When collisions distribute the originally excited molecules among various rotational or vibrational upper states, the spectral distribution of the fluorescence broadens. With some other collisions, all or most of the excitation energy can be degraded in a non-radiative process. This latter phenomenon reduces the fluorescence intensity and is, therefore, referred to as quenching. Thus, the fluorescence intensity depends upon the pressure, temperature and nature of the gas. Therefore, the partial pressure of all molecular species present in the sample volume,as well as the rate constants for the deactivation of the studied excited state,must be known before LIF can be used effectively for quantitative measurements.

2 - FLAMES STUDIES BY L.I.F.

The availability of tunable dye lasers has markedly enhanced the ability to inquire into the chemistry and physics of combustion systems,and now makes LIF well suited for the study of trace compounds in complex combustion media.

A spectroscopic study of CH, OH, C_2 and CN by LIF in two analytically useful flames such as air-acetylene and nitrous oxide-acetylene has been done by Fujiwara et al [3]. In this work, laser excited background molecular fluorescence may interfere with the signal of atomic fluorescence.

An application of LIF to a study of the chemistry of sulfur in rich hydrogen/oxygen/nitrogen flames has been carried out by Muller et al [36] ; this work demonstrates a simple procedure for taking quenching effects into account. Fluorescence measurements of S_2, SH, SO_2, SO and OH concentration as well as H-atom densities (in sulfur-free flames), along with measurements of flame temperature have been employed to develop a kinetic model for the highly coupled flame chemistry of sulfur. Several studies have been performed on the hydroxyl radical in flames

[37] ; Cottereau et al [38] have performed an investigation of low pressure flames with short duration laser pulses in order to obtain both a direct measurement of the quenching rate under various experimental conditions and the direct local OH concentration in a single pulse.

Grieser et al [39] have demonstrated that laser fluorescence can be used to detect NO in atmospheric-pressure flames. Laser fluorescence techniques for NO are of interest for studying the mechanisms of NO formation and its influence on chemical processes and polluant formation in flames.

Finally LIF spectroscopy is being developed as an in-situ, real time diagnostic for polycyclic aromatic hydrocarbons in combustion systems [40]. They are known to be formed in sooting flames and are of interest both for their carcinogenic properties and possible role in the soot formation process.

3 - FLOWFIELD INVESTIGATION BY L.I.F.

A practical application has been carried out at ONERA in a hot subsonic jet which was produced by combustion of jet fuel and has a mass flow rate of about 1 kg/s. The purpose was to study the noise emission of the jet in relation to acoustic studies.

In the course of preliminary Raman scattering work on the jet a considerable spurious fluorescence emission,for a flow temperature up to 900 K,had precluded any detection of Raman lines,using an argon ion laser as the source. It was thus proposed to use these naturally present fluorescent components as tracers of the combustion products [18]. A preliminary work was done in order to :

1) study the influence of the jet temperature,
2) monitor homogeneity of the spatial distribution of the fluorescent species in the jet. Then,a comparison with the spatial distribution of a well known combustion product such as CO_2 was done in order to check that nearly no quenching effects occurs.

Density fluctuation studies have been carried out on the fluorescence products of the jet. Finally, some other fluorescent molecules which can be introduced into any kind of jet are presently being searched.

a - Experimental arrangement

Figure 3 presents the experimental set up used for the investigation of the jet. The argon ion laser beam is focused into the jet, to a small volume of about 1 mm^3, and appropriate optics collect the emitted fluorescence at right angle from the laser beam axis. The spectral discrimination is accomplished through colored filters absorbing the background radiation due to Mie and Rayleigh scattering (at the incident wavelength). The fluorescence signal is detected by a photomultiplier. The output signal from the photomultiplier is amplified, digitized and processed by a computer.

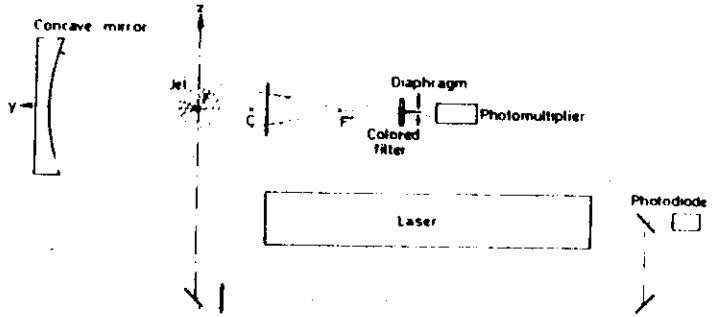

Fig. 3 - Experimental arrangement for laser-induced fluorescence.

b - Results

The fluorescence intensity increases with the burner temperature up to 900 K and then decreases rapidly. Therefore, all measurements are done at 900 K (Fig. 4). Jet profiles of the spatial distribution of the fluorescence intensity have been recorded and show that the fluorescent species are evenly distributed across the jet. Fluctuation spectra of the fluorescence intensity (Fig. 5) are drawn for several spatial positions in the jet. They show that the amplitude of the turbulence is smaller in the center of the jet.

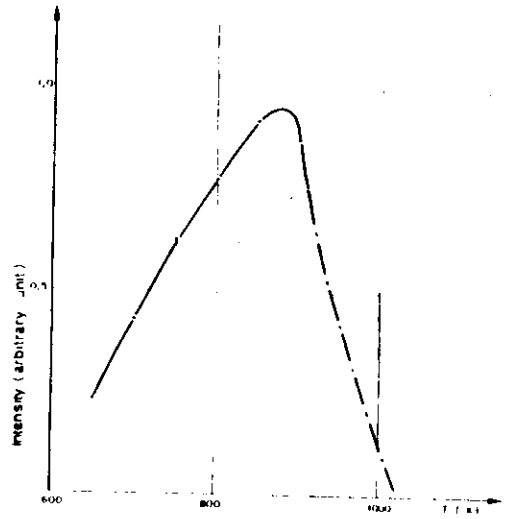

Fig. 4 - Fluorescence intensity as a function of temperature.

Finally, a correlation was made between the fluorescence signals emitted at different axial positions in the jet and the output of a fixed infrared radiometer monitoring the emission from an axial position. The times at which the maxima occur in the correlation function (Fig. 6(a)) are drawn as a function of the distance between the volumes probed by fluorescence and by radiometry. A straight line is obtained (Fig. 6(b)), the slope of which gives the convection velocity.

4 - SATURATED LASER FLUORESCENCE IN COMBUSTION STUDIES

A barrier to the quantitative application of fluorescence to species analysis in flames has been the need of preliminary informations about quenching effects. However, by solving the rate equations for the system, it can be shown that when the power density of the laser is high enough to saturate or nearly saturate optical transitions, the fluorescence intensity becomes independent of the laser intensity, quenching rates and fluorescence lifetime.

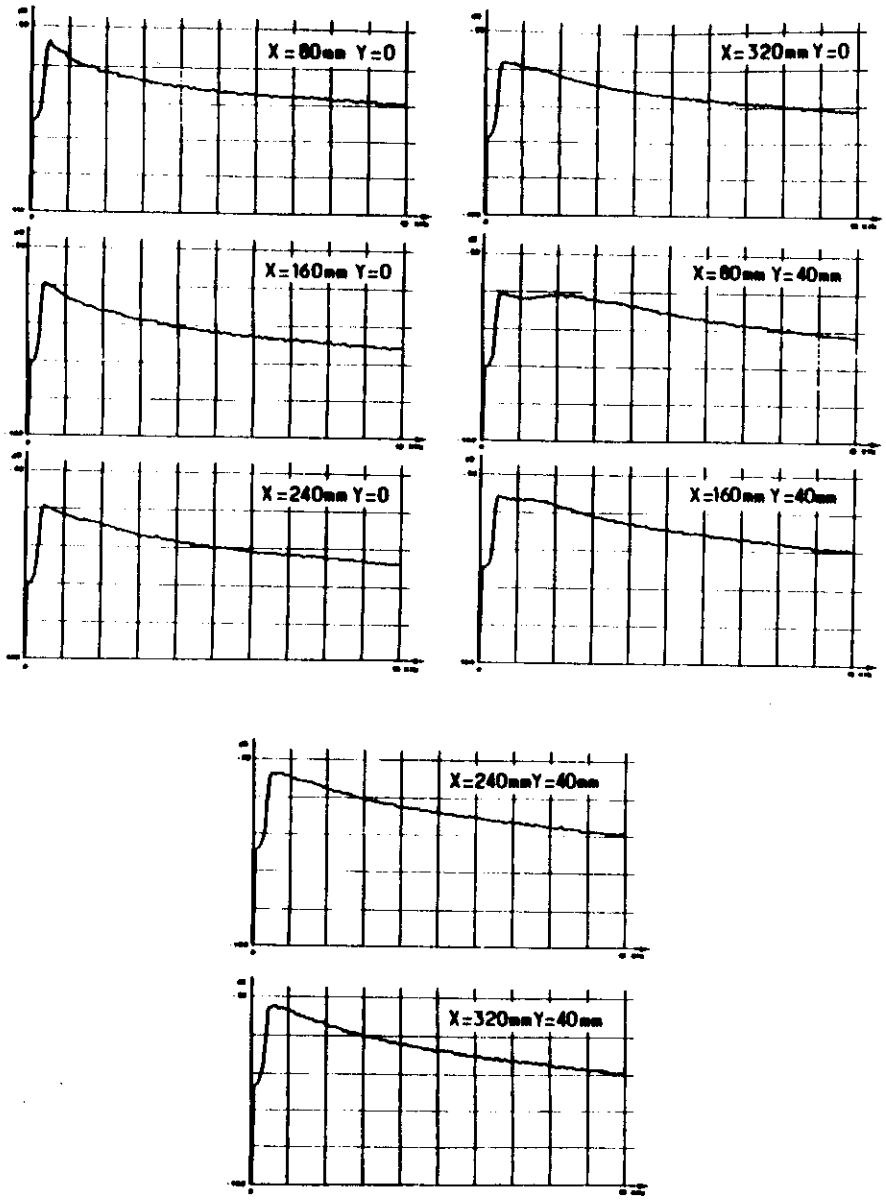

Fig. 5 - Fluctuation spectra of the fluorescence intensity for different axial and radial positions in the jet.

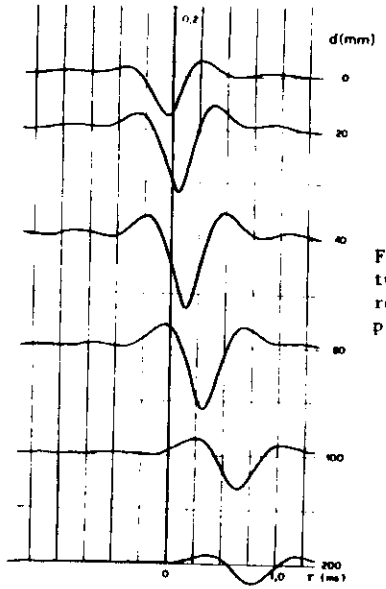

Fig. 6(a) - Correlation profiles between radiometry and fluorescence measurements ; d is the distance between the probed volumes on the X axis (mm).

Fig. 6(b)

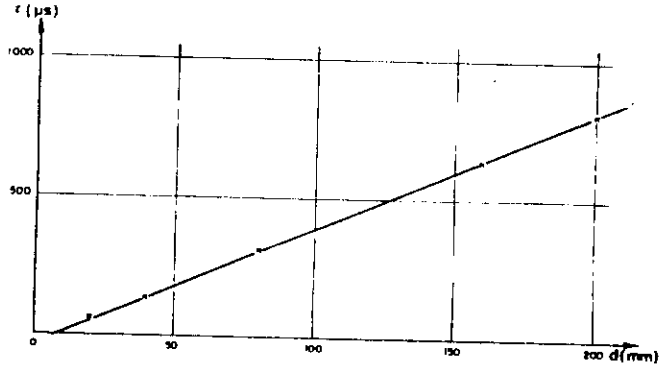

This approach to avoid the quenching problem was put forward by Piepmeir [41]. Theoretical developments have been made by Daily [5, 42, 43]. Successful application of the technique to flame radicals such as CH, OH, C_2 and CN have been demonstrated [19, 20, 44-46]. In practice, it may be very difficult to saturate fully, since the rate of quenching is generally large in flames. However, it has been shown by Baronavski and Mc Donald [19, 20] that if the laser beam is focused to a small cross sectional area in order to reach partial saturation, then a measurement of fluorescence power versus laser spectral intensity yields the total quenching rate together with the number density.

The saturation fluorescence technique is not applicable to all molecular species. There are specific criteria which must be met. The molecule must first of all have a known emission spectrum. Moreover, it is necessary to tune the laser to a suitable molecular absorption wavelength. With the lasers which are available today, it is possible to study several molecules of interest for combustion diagnostics ; the most important of these molecules are listed in table I. The use of saturated fluorescence eliminates or at least reduces the problem of quenching,and has the further advantage that the fluorescence intensity becomes insensitive to variations in laser power. However, the generation of high concentrations of excited states under saturated excitation,in an active flame environment,opens up the possibilities for laser induced chemistry effects that also must be taken into account or avoided [36]. Saturated fluorescence measurements have been applied to minor constituents such as OH and C_2 in a Bunsen flame [48] or CH and CN in an homogeneous flame (in order to make comparison between absorption and fluorescence) [46]. OH has been selected by several groups for saturated fluorescence studies [47, 49, 50] . Reference [49] gives a multilevel model of response to laser excitation and in reference [50],a Nd : YAG pumped dye laser is used to excite an isolated rotational transition of OH. The resulting fluorescence signal is analysed,both spectrally and temporally,in order to study the development of the excited state rotational distribution.

TABLE I - ELECTRONIC TRANSITIONS OF SOME MOLECULAR RADICALS

MOLECULE	λ(Å)	ELECTRONIC TRANSITION
NO	2270	$A^2\Sigma^+ \leftarrow X^2\Pi$
OH	3064	$A^2\Sigma^+ \leftarrow X^2\Pi$
NH	3360	$A^3\Pi_i \leftarrow X^3\Sigma^-$
CN	3883	$B^2\Sigma^+ \leftarrow X^2\Sigma^+$
CH	4315	$A^2\Delta \leftarrow X^2\Pi$
C_2	5165	$d^3\Pi_g \leftarrow a^3\Pi_u$

These wavelengths correspond to the bandhead positions, which are particularly well-defined spectral feature in the rotational lines structure [51].

II - SPONTANEOUS RAMAN SCATTERING

1 - INTRODUCTION

The Raman effect is a light scattering phenomenon which takes place in a material medium and whereby the scattered light undergoes a wavelength change,and the scattering molecules an energy change. This process is illustrated in Fig. 7. Figure 1 shows a typical experimental arrangement for which both spontaneous Raman scattering and LIF can be observed. The scattered light intensity for the Raman process can be expressed by :

$$P_{scatt.} = P_L \times N \times \frac{d\sigma}{d\Omega} \times \ell \times \Omega$$

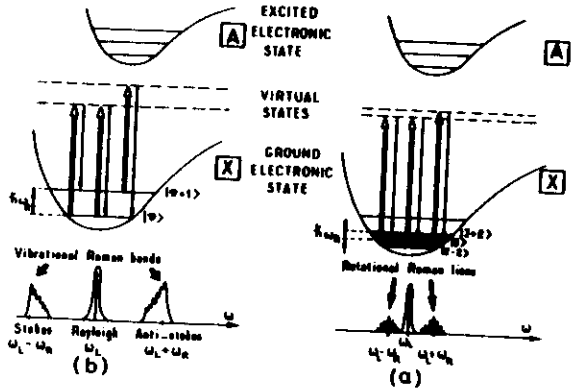

Fig. 7 - Energy level diagram of the rotational (a) and vibrational (b) Raman process, and resulting spectra.

where N is the number density of scattering molecules in the initial level ; the other parameters are defined in Fig. 1.

Two important differences must be pointed out :

- Raman scattering is a very weak process compared to fluorescence, since its scattering cross-section is ten orders of magnitude smaller (see introduction),
- the term "scattering" is used to designate a re-emission process which is effectively instantaneous,whereas fluorescence process is characterized by a significant time delay.

During the scattering process, there is also a possibility that no exchange of energy takes place between the incident light and the molecules ; the process is then called Rayleigh scattering. Quantum theoretically, the incident photons collide elastically or inelastically with the molecules, to give Rayleigh and Raman lines respectively ; the inelastic process is much less probable than the elastic one.

When an inelastic collision occurs between a molecule in its ground state and the incident photon, energy is supplied to the molecule which is thus raised to a higher energy level. The scattered photon is of lower energy and gives rise to what is called the Stokes line. If the scattering molecule is initially in an excited state and gives up energy to the impinging photon thus moving to a lower energy state ; the scattered photon gives rise to the anti-Stokes line.

Because of energy conservation, the energy of the scattered photon is equal to $\hbar\omega_L$ (incident photon) plus or minus the energy gap $\hbar\omega_R$ between the initial and the final states of the scattering molecule (ω is the angular frequency). A Raman spectrum is thus composed of two symmetrical bands which are shifted with respect to the incident light frequency. Since the anti-Stokes line must originate from molecules of higher energy, which are less abundant in a medium at Boltzmann equilibrium, the anti-Stokes lines are expected to be weaker than the Stokes lines.

2 - SPECTRAL PROPERTIES

The vibrational and rotational quantum numbers of the initial state of the molecule are called v and J respectively. As pointed out from the former discussion, the energy state of the molecule is changed through a Raman scattering process ; v and/or J quantum numbers are thus different in the final state. Consequently, there are two different groups of Raman spectra : pure rotational and vibrational as illustrated in Figs. 7(a) and (b) respectively. In the first case,only the J value is changed after the transition,whereas both v and J change in the last case.

The rotational Raman spectrum is governed by a selection rule applied to each individual rotational transition, namely :

$$\Delta J = 0, \pm 2 \qquad (1)$$

$\Delta J = 0$ corresponds to the undisplaced line (Rayleigh scattering). The transition $J \rightarrow J+2$ results in a shift to longer wavelengths (Stokes lines) and the transition $J+2 \rightarrow J$ results in a shift to shorter wavelengths (anti-Stokes lines).

The rotational term values for diatomic molecules are represented by the expression :

$$\frac{E(J)}{hc} = F(J) = B\,J(J+1) - D\,J^2(J+1)^2 \qquad (2)$$

where h is the Planck's constant, c is the light velocity, E(J) is the rotational energy, B and D are the rotational constant and the centrifugal distortion constant respectively.

Using Eq. (2), the magnitude of the frequency shift for both Stokes and anti-Stokes transitions can be found :

$$F(J+2) - F(J) = (4B - 6D)\left(J+\frac{3}{2}\right) - 8D\left(J+\frac{3}{2}\right)^3 \qquad (3)$$

Equation (3) gives the positions of the series of rotational Raman lines on either side of the Rayleigh line ; these lines constitute the pure rotational Raman spectrum.

The vibrational selection rules for the vibrational Raman spectrum of an oscillator are :

$$\Delta v = \pm 1 \qquad (4)$$

The term value for the anharmonic vibrating rotator is given by :

$$T = G(v) + F(J) = \omega_e\left(v+\frac{1}{2}\right) - \omega_e x_e\left(v+\frac{1}{2}\right)^2 + \omega_e y_e\left(v+\frac{1}{2}\right)^3 + B_v\,J(J+1) - D_v\,J^2(J+1)^2 \qquad (5)$$

where :

- ω_e is the vibration frequency of the oscillator with nuclei in the equilibrium position,
- $\omega_e x_e$ and $\omega_e y_e$ are the anharmonicity constants,
- $B_v = B_e - \alpha_e\left(v+\frac{1}{2}\right)$ (6a)
- $D_v = D_e + \beta_e\left(v+\frac{1}{2}\right)$ (6b)
- α_e and β_e are the rotation-vibration coupling constants.

The Raman spectrum of the vibrating rotator governed by the vibrational selection rules $\Delta v = \pm 1$ and rotational selection rules $\Delta J = 0, +2, -2$ consists of three vibrational branches which are called Q, S and O respectively. Because of the anharmonicity of the vibration and of the coupling between rotation and vibration, each rovibronic level of the ground electronic state of the molecule gives rise to a particular set of distinct Raman lines.

The Raman shifts can be represented by the equation :

$$T' - T'' = \Delta\omega_0 + B'_v J'(J'+1) - B''_v J(J+1) - D'_v J'^2(J'+1)^2 + D''_v J^2(J+1)^2 \qquad (7)$$

with $\Delta\omega_0 = G(v') - G(v) = \omega_e(v' - v) - \omega_e x_e (v'^2 - v^2 + v' - v) + \{v'^3 - v^3 + \frac{3}{2}(v'^2 - v^2) + \frac{3}{4}(v' - v)\} \omega_e y_e$

Neglecting the centrifugal distortion constants, the following equations are obtained for the O, S and Q Raman shifts :

$$\Delta T(O) = \Delta\omega_0 + 2B'_v - (3B'_v + B''_v)J + (B'_v - B''_v)J^2 \qquad (8a)$$

$$\Delta T(S) = \Delta\omega_0 + 6B'_v + (5B'_v - B''_v)J + (B'_v - B''_v)J^2 \qquad (8b)$$

$$\Delta T(Q) = \Delta\omega_0 + (B'_v - B''_v)J(J+1) \qquad (8c)$$

For a cold vibrational transition (originating from $v = 0$), the difference between B_v' and B_v'' is very small. The lines of the Q branch are, therefore, very close to each other and are usually not resolved, giving rise to a compact and intense Q branch. The S and O branches appear much weaker since their lines are note superimposed.

An advantage of SRS lies in the fact that homonuclear diatomic molecules, which are infrared inactive, are Raman active and can be easily analysed. At this point, a few words should be said about the classification of molecules into groups. Molecules are classified according to the relative values of their three moment of inertia. Those possessing three different moments of inertia are referred to as asymmetric top. If all three moments of inertia are equal, the molecule is called a spherical top, and if only two moments are equal but the third is different, the molecule is referred to as a symmetric top. These may be further divided into prolate for which $I_A < I_B = I_C$ and oblate for which $I_A > I_B = I_C$. If $I_A = 0$, the molecule is a linear molecule, which is a special case of

prolate symmetric top. Linear molecules may have a center of inversion ; they then belong to $D_{\infty h}$ point group ; a molecule that does not have a center of inversion is referred to as belonging to point group $C_{\infty v}$ [51].

Molecules having a center of inversion do not have a permanent dipole moment and, therefore, do not have a pure rotational infrared spectrum. The same is true for spherical top molecules. The asymetric top molecules whose moments of inertia are all different, do possess a pure rotational infrared spectrum. However, all molecules except spherical tops, irrespective of their symmetry, do have a pure rotational Raman spectrum.

In the case of Raman spectra, the amplitude of the dipole moment induced by the incident radiation must change during the transition. According to the Placzek polarisability theory [12, 13], the amplitude of the induced dipole moment for a molecule is given by :

$$\underline{\mathcal{P}} = \alpha \underline{E} \qquad (9)$$

where α is the molecular polarizability and E the electric vector of the incident radiation of frequency ω_L. The polarizability α can be developed as a function of the normal coordinate of vibration q :

$$\alpha(t) = \alpha_0 + \left.\frac{\partial\alpha}{\partial q}\right|_0 q(t) \qquad (10)$$

In a non-symmetric molecule, a periodic change of the polarizability takes place during all normal vibrations. The induced dipole changes and the molecules are, therefore, Raman active. For symmetrical molecules this is not always the case although it is possible for a linear symmetrical molecule to he infrared inactive and Raman active. It should be noted here that all homonuclear diatomic molecules like O_2, N_2, H_2 etc... are infrared inactive while they are all Raman active. This is a result of the fact that the dipole moment and its change are zero for them, whereas their polarizability α, its change $\partial\alpha/\partial q$ and the resulting amplitude change in the induced dipole moment do not vanish. This description of the Raman and infrared activity of the molecules is of a very elementary nature ; detailed treatments of the subject can he consulted in refs [9, 12, 13, 51].

3 - LINE INTENSITIES OF ROTATIONAL AND VIBRATIONAL RAMAN SPECTRA

One of the fundamental mesurable quantities of interest for the applications considered is the intensity of a given line. For a theorical determination of the intensity of a spectral line, it is necessary to know the distribution of the molecules in the various initial states and the corresponding transition probabilities [51].

a - Population distribution

According to the Maxwell-Boltzmann distribution, the number of molecules in each of the vibrational states is proportional to :

$$N_v \propto e^{-\frac{G(v)hc}{kT_v}} \qquad (11)$$

where k is the Boltzmann constant and T_v the vibrational temperature.

In order to obtain the number of molecules in a particular energy level referred to the total number of molecules N, the state sum or partition function

$$Q_v = \sum_v \exp\left(\frac{G(v)hc}{kT_v}\right) \qquad (12)$$

must be utilized.

The number density of molecules in the state v is therefore,

$$N_v = \frac{N}{Q_v} \exp\left(\frac{G(v)hc}{kT_v}\right) \qquad (13)$$

The number of molecules N_J in the rotational level J is proportional to :

$$N_J \propto (2J+1)\exp\left(\frac{F(J)hc}{kT_R}\right) g_J \qquad (14)$$

where :

- T_R is the rotational temperature,
- g_J is the weighting factor due to the nuclear spin function,
- the level (J) has a $(2J+1)$-fold degeneracy in the absence of an external field

It is seen that N_J goes through a maximum as we increase J. This maximum is found for $J_{max} = \left[\frac{kT_R}{2Bhc}\right]^{1/2}$

In an analogous way as in the vibrational state, one also makes use of a rotational partition function Q_R so that one has :

$$N_J = \frac{N}{Q_R}(2J+1)\exp\left(-\frac{F(J)hc}{kT_R}\right) g_J \qquad (15)$$

At this point, from eqs (14) and (15), we note that the intensity of each line is proportional to the number density N and that the dependence of intensity upon temperature is given by a known function :

$$f(T) = \frac{2J+1}{Q_R Q_v} \exp\left\{-\frac{(G(v)+F(J))hc}{kT}\right\} g_J$$

with $T_R = T_v = T$.

Due to the very small differences in the wavelengths of the rotational lines, in particular when a mixture of gases is involved, the resolution sometimes is insufficient to separate the contributions of the various species. Therefore, vibrational Raman scattering, which permits clear identification of species since the vibrational Raman shifts of the various constituents are generally quite different, is more advantageous to use. In the following, the discussion will therefore be restricted to this process. We note in passing that the o and s branches, as mentioned above, are much weaker than the Q-branch. They are therefore of minor importance as far as application to gases are concerned, and they will be neglected in the following.

b - Raman line intensities

The Q-branch, if a highly dispersive instrument is used, can be resolved into components corresponding to the energy levels characterized by the excited vibrational quantum number $v = 1, 2, \ldots$. These, of course, will appear at high temperatures in bands which are called "hot bands" and may be used to determine temperature as will be discussed later.

The intensity of the scattered light for a line of the Stokes Q-branch is given by :

$$P_S(v, J \rightarrow v+1, J) = N P_L\left(\frac{d\sigma}{d\Omega}\right)_S f(T) \times \Omega \times \ell\,(v+1) \qquad (16)$$

and for a line of the anti-Stokes Q-branch by :

$$P_{AS}(v, J \rightarrow v-1, J) = N P_L\left(\frac{d\sigma}{d\Omega}\right)_{AS} f(T) \times \Omega \times \ell \times v \qquad (17)$$

where :

$\left(\frac{d\sigma}{d\Omega}\right)_{S \text{ or } AS}$ are the differential cross sections for the Stokes and anti-Stokes branches respectively. They are proportional to ω_S^4 and ω_{AS}^4 respectively, where ω_S and ω_{AS} are the frequencies of the Stokes and anti-Stokes lines,

$\nu + 1$ and ν are derived from the transition moments which are enclosed in the numerators of the scattering cross section.

The remaining parameters are presented in Fig. 1. Eqs (16) or (17) show that the ratio of the intensities of two suitably chosen lines (or integrated intensities of two bands) is independent of the number density and temperature can thus be obtained. Once the temperature is known, the number density can be obtained from the measurement of the intensity of one line (or from the integrated intensity of one band).

Any set of lines can be used to measure temperature. However, this set of lines should be selected in order to maximize signal to noise ratio and accuracy of measurement. The purpose of the next section is to give simple rules for the selection of the best procedure.

4 - METHODS USED TO DETERMINE THE TEMPERATURE

Several approaches can be used in order to determine the temperature. Setchell [31] has measured it from the relative intensities of the Stokes lines of hydrogen and also from the ratio of the intensities of the hot Stokes band to the cold Stokes band of nitrogen. On the other hand, Lederman [30] has used Stokes and anti-Stokes bands. However some general rules must be outlined.

The set of bands or lines to be used depends on the range of temperatures expected. Figure 8 shows the fraction of nitrogen molecules in the $\nu = 0$ and $\nu = 1$ energy states as a function of temperature. When the temperature is low (< 1000 K), the fraction of molecules in excited vibrational states is insufficient to permit the use of the anti-Stokes Q-branch ($\nu = 1 \rightarrow \nu = 0$) or of the hot Stokes Q-branch ($\nu = 1 \rightarrow \nu = 2$). Temperature is, in this case, best measured from the relative intensities of the rotational lines of the cold Q-branch ($\nu = 0 \rightarrow \nu = 1$). These lines have a spacing of about 1 cm^{-1} for nitrogen , but it is not necessary to resolve the branch as the analysis of the shape of its envelope is generally sufficient. Figure 9 is an illustration of the Stokes Q-branch profiles for nitrogen at 293 K and 1000 K.

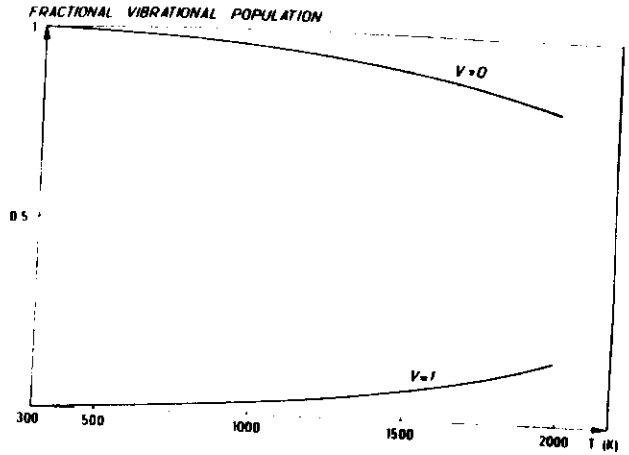

Fig. 8 -Fraction of nitrogen molecules in V=0 and V=1 states.

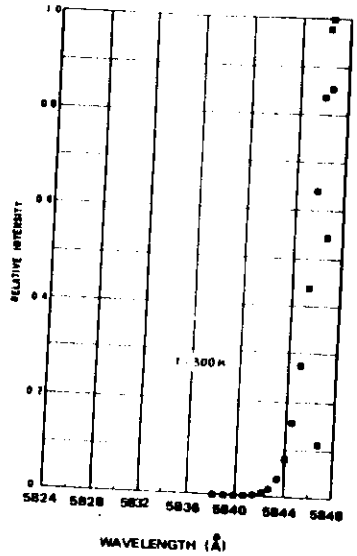

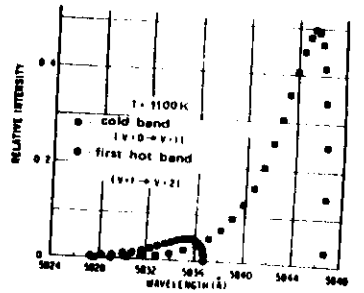

Fig. 9 - Rotational structure of the fundamental stokes Q branch of nitrogen for even values of rotational quantum number J at room temperature and 1110 K from [26]

Two methods are available at higher temperatures ; they both require the presence of molecules in an excited vibrational state. More than 10 % of the molecules are in the $\nu = 1$ level for species like nitrogen or oxygen when the temperature exceeds 1500 K. Temperature may then be obtained from the ratio of the measured Raman Stokes and anti-Stokes Q-branch integrated intensities (Fig. 10). Equations (16) and (17) lead to :

$$\frac{P_S}{P_{AS}} = \left(\frac{\omega_S}{\omega_{AS}}\right)^4 \exp\left(\frac{\hbar \omega_q}{k T}\right) \qquad (18)$$

The latter can be rewritten in a different way in order to give temperature :

$$T = \frac{\hbar \omega_R}{k} \left(\text{Log} \frac{P_S}{P_{A.S}} + 4 \text{Log} \frac{\omega_S}{\omega_{A.S}} \right)^{-1} \qquad (19)$$

It appears from Fig. 10 that this method is applicable above 1000 K.

It is also possible to measure the temperature from the ratio of intensities of the first hot band to the cold band or from the ratio of two consecutive hot band intensities (second and first, third and second...).

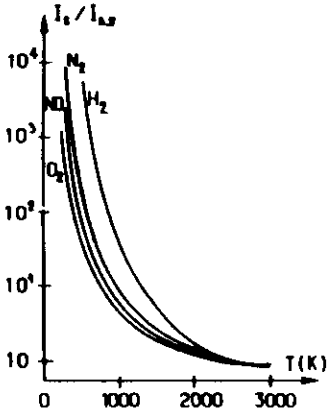

Fig. 10 - Ratio of stokes to anti-stokes Raman intensity as a function of temperature.

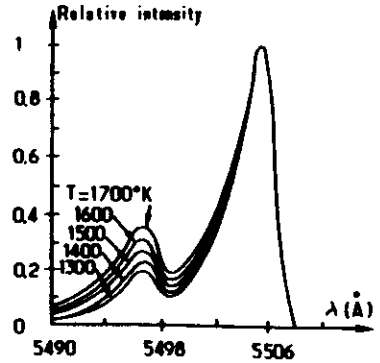

Fig. 11 - The resolved Q branch of nitrogen, from [26]

Two comments must be made :

1. - The first method, because it is based on rotational structure, gives the rotational temperature while the two others give the vibrational temperature. These two temperatures are generally equal, unless equilibrium conditions do not prevail (e.g. in a discharge).

2. - When the vibrational temperature is high enough, both vibrational and rotational temperatures can be simultaneously measured [52].

5 - BACKGROUND SIGNALS

SRS is a weak process, so that any background light leads in general to very poor signal to noise ratio. Background interference may arise from room lighting, chemiluminescence or laser-induced processes such as Rayleigh and Mie scattering, fluorescence or blackbody emission of particles heated by chemical reaction or by the laser.

The total number n of photoelectrons detected over a given time interval obeys Poisson statistics. The fluctuation about the mean value n is given by the standard deviation $\sqrt{n}$. But n is actually made up of two parts :

$$n = n_S + n_B$$

where n_S is the number of signal photoelectrons whereas n_B is the number of background photoelectrons. The signal to noise ratio can therefore be described by the following expression :

$$\frac{S}{N} = \frac{n_S}{\sqrt{n}} = \frac{\sqrt{n_S}}{\sqrt{1 + n_B/n_S}}$$

It is important to note that although the noise n_B is substracted from n in order to retrieve n_S, S/N can be considerably degraded by the presence of n_B. Thus, to obtain the best S/N, n_B must be minimized. Several of these background sources that can be encountered are discussed below ; they are classified in three groups :

1 - Laser-induced background emissions (Rayleigh, Mie, fluorescence), scattering by windows, etc. Apart from fluorescence, these emissions are not very hard to reduce or eliminate since they are spectrally well separated from the Raman signal. With a rejection of 10^{-14}, which can be obtained by an efficient monochromator and filters, these background signals can, in general, be completely eliminated. The problem of fluorescence (from windows or from the system under study) is more delicate because this noise may occur at the same wavelength as the Raman line. Two methods could be used to circumvent the problem of fluorescence background :

(i) with CW lasers by wobbling the output slit at a fixed rate and employing phase - sensitive detection, similar to the technique employed for the detection of weak infrared absorption lines of pollutants. This only works if the fluorescence background has a broad and unresolved spectral feature.

(ii) polarization modulation of the laser light (which causes a modulation of the Raman light entering the spectrograph [53]), with phase sensitive detection ; the fluorescence which is unpolarized is here discriminated against.

2 - Noise signals such as gas luminosity, ambient light and dark current of the photomultiplier. Because these signals are independent of the laser power, their contributions can be easily reduced by using pulsed lasers in conjunction with time-gated electronics.

3 - Laser-induced particle incandescence. This noise is only observed when pulsed lasers are used. It is due to the black-body emission of particles heated by the incident beam. S/N can be increased by using very high power pulsed lasers [54] but a simpler solution will be proposed below.

From the above, it is evident that the problems which arise with CW and pulsed lasers are quite different. Quantities measured depend also upon the choice of the laser source.

6 - APPLICATION TO FLOWFIELD AND COMBUSTION DIAGNOSTICS

Different techniques have been used to study turbulent media in the last years.

M. Lapp and his group, using a C.W. Argon/ion laser, applied vibrational Raman scattering to the measurement of concentration and temperature. They have used the resolved Q-branch intensity profile to the measurement of temperature in a flame [26]. Some recent results have been reported by Drake et al [55], Warshaw et al [56] and Lapp [57, 58] in which the thermodynamic and flowfield properties of an H_2-air co-flowing jet turbulent diffusion flame have been measured. Stokes to anti-Stokes intensity ratio for N_2 were used to determine temperature, whereas the concentration of N_2, H_2 and H_2O were evaluated from the Stokes signal intensity following a calibration. A pulsed dye laser source producing 1 J pulses at repetition rates up to 1 pulse/s was used.

Lederman et al [30, 59, 61] have been active in the field of laser Raman diagnostics for a number of years. They use a 150 MW Q-switched Ruby laser, capable of providing six pulses per minute with a pulse half-width shorter than 20 ns. This source has been used to obtain data on several systems. The first one was a coaxial air-CO_2 mixing jet where concentration of CO_2 has been obtained. The second was an air-methane-CO_2 flame were concentration of species and temperature has been measured and the third a simulated internal combustion system in which the temperature and concentration of species has been demonstrated to be measurable.

Williams et al [62] have also used both Q-switched and free-running modes of a ruby laser to study the turbulent mixing region of a rocket plume. Time averaged temperatures, obtained from the pure rotational branches, range from 900 K to 1800 K, with H_2, O_2, CO and CO_2 number density being between 10^{17} and 10^{19} cm^{-3}.

Two particular problems deserve further discussion :

1. - When the system under study contains particulate matter, laser-modulated particulate incandescence occurs (as discussed in 5.3). The soot particles absorb the incident laser radiation, are heated up to temperatures far above the ambient flame temperature and, thereby, emit greatly increased amounts of blackbody radiation. This phenomenon may prevent detection of Raman emission ; for example, Eckbreth has shown that signal to noise ratios as low as 10^{-2} to 10^{-4} can occur in hydrocarbon flames for a laser power density of 10^6 W/cm^2.

2. - Only mean values and statistical distributions are obtained from signal averaging over several pulses. This is due to the low repetition rate of pulsed lasers ; these repetition rates are in the range of 1 to 100 pulses per second.

This difficulty must be circumvented in order to perform time-resolved measurements, e.g. for studies of turbulent media. Therefore, 1 mm spatial resolution and 10 μs response time must be achieved. For typical combustions, the averaged power of the laser source must be 50 kW over periods as long as possible. Free-running ruby lasers, which provide up to several tens of joules over periods of 1 ms are suitable for this purpose.

Figure 12 presents the experimental arrangement used at ONERA to evaluate the potential of such a technique [63]. The ruby laser, which normally emits 30 joules, is used here in an intracavity configuration. For this application, the output mirror M_2 has been replaced by

an afocal system composed of a 23 cm focal length lens L and a concave mirror M_3 having 25 cm radius of curvature. The net two-way energy available for Raman scattering is then about 100 J in 700 µs.

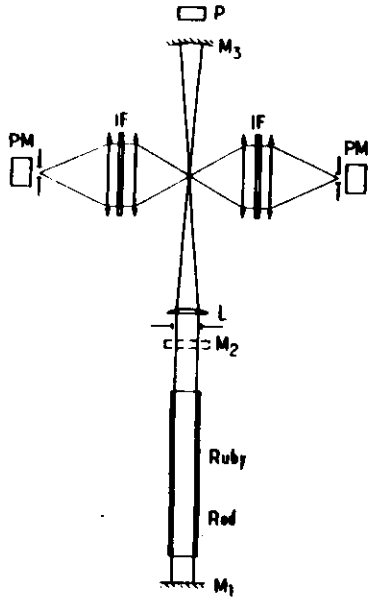

Fig. 12 - Experimental arrangement for SRS measurement with a pulsed laser.

The light scattered from the 1 mm long by 200 µm diameter focal volume is collected by two sets of f/1 AR coated optics, oriented at 90° with respect to the laser beam. One channel collects the Stokes emission from N_2 at 828.4 nm, the other one the anti-Stokes line at 597.6 nm. The Stokes line is filtered by an interference filter of 2.4 nm width and 6 mm of Schott RG 780 glass, and then detected by means of an RCA 8852 phototube ; the anti-Stokes emission is isolated by interference (3.5 nm width) and wide band pass dichroic filters, and then detected by an RTC XP 1003 tube. The Raman signals are displayed on a scope screen together with the photocurrent delivered by the diode that monitors the laser power. RC circuits with a time constant of about 15 µs provide integration over 30 or so laser spikes.

A 24 mm diameter premixed H_2/O_2 burner was selected for the present work in order to obtain temperatures in the range of 1500 K to 2000 K, and to avoid laser-induced particle incandescence problems. N_2 was added as the Raman scatterer and a cross flow of cold gas through a small horizontal nozzle can be supplied in order to create turbulence in the sample volume. This gas can be either reactive (O_2, H_2) or unreactive (N_2, CO_2, H_2).

Before performing measurements of turbulence, it was verified that all sorts of noise were eliminated or sufficiently reduced, except laser-induced particle incandescence which only vanishes when clean gases are blown through the probe volume. However, it has been found that these particles can be burnt up and ejected in a few microseconds irrespective of their number and size. This is evidenced in the scope traces of figure 13. These recordings were obtained in room air and are quite typical. For STP conditions, an anti-Stokes signal can not be detected with our apparatus. A signal appears however on the anti-Stokes channel ; it is due to laser-induced particle incandescence. The anti-Stokes channel is more affected by the presence of particles due to its higher gain and because the high temperature of the particle surface (> 4000 K) causes more radiation to be emitted into its bandwidth than on the Stokes side. One sees that the burst of particle radiation lasts no more than 50 µs. This is verified even in the presence of heavy particles. Possible explanations for these observations are based on particle ablation or ejection.

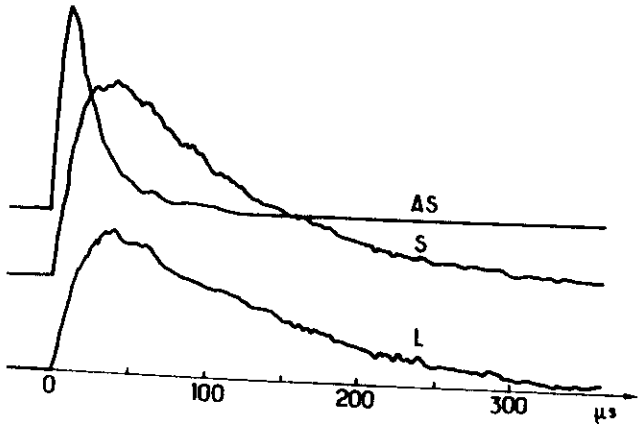

Fig. 13 - Scope traces of laser (L) and Raman (A.S. and S) intensities obtained in air at STP.

The particle radiation thus disappears rapidly. By time gating out the initial 50 µs, the disturbing influence of particles can be practically eliminated with free-running ruby laser pulses. If the flow is sufficiently slow, e.g. 0 to 10 m/s, particles entrained are kept from penetrating deeply into the focal region and from causing any disturbance.

Measurements were then performed in the stable flame $H_2 + O_2 + N_2$. The traces of figure 14 were obtained at about 1500 K and 50 % N_2. Although stable conditions prevailed, small oscillations of 10 % amplitude or less are observed for temperature measurements when they are obtained from the anti-Stokes to Stokes ratio. These fluctuations are real, since

our measurement accuracy is on the order of 3 % for these conditions, given the laser power, N_2 number density and PM quantum efficiency.

Finally, figure 15 presents a typical set of traces observed in the mixing zone with CO_2 injection. This was obtained with a 7 µs time constant. Strong turbulence is observed, with temperature variations as large as 30 % peak to peak, associated with comparable density fluctuations on a time scale of 50 µs.

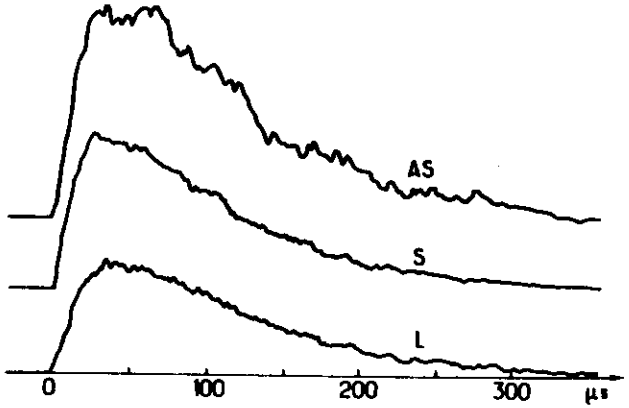

Fig. 14 - Scope traces of laser and Raman intensities obtained in the stable flame at about 1500 K and 50% of N_2.

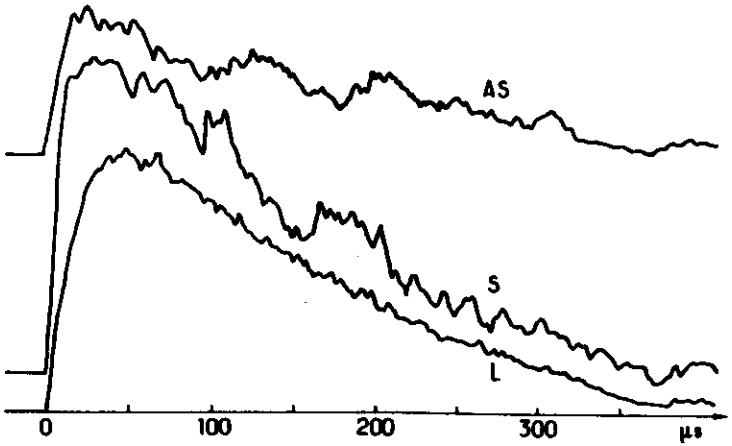

Fig. 15 - Scope traces of laser and Raman intensities observed when a CO_2 flow is injected near the probe volume.

III - COHERENT ANTI-STOKES RAMAN SCATTERING

This technique is based on a four wave mixing process and is one of the many well-known third-order nonlinear optical processes. CARS offers an attractive alternative to conventional Raman spectroscopy, its superiority coming from its coherent nature.

CARS has been first applied to crystal spectroscopy [64-66] and to the measurement of third-order susceptibilities in gases [67-69]. Then, it has been used for point non-intrusive diagnostics in various flames [70-76] and recently in combustors of practical interest [77-80] ; it has also proved successful for studies of low-pressure gases, discharges or plasmas [81, 82]. Broadband multiplex CARS is an interesting development of the method for obtaining instantaneous temperature and concentration measurements [83, 84]. High resolution Raman spectroscopy is another application of CARS which shows great promise. Using CW lasers, it has been applied to ultra high resolution work in gases [85-87]. High resolution vibrational [88] and rotational [89] CARS spectra were also obtained in gases with high power pulsed sources. CARS has been used with picosecond lasers to study relaxation mechanisms [90].

CARS has also allowed the observation of fluorescence free resonant Raman spectra in liquid biological samples [91, 92] as well as in gases [93, 94]. Recently, the theory of resonant CARS in the limit of Doppler broadening has been developed [95].

The theoretical understanding of third-order nonlinear processes and of CARS in particular is presented in the first part of this chapter. A classical approach is used to introduce the basic equations of the interaction process. However, the quantum mechanical treatment leads to the proper expression of the nonlinear susceptibility. The latter is obtained by conventional perturbation theory or by means of a time ordered diagrammatic representation and its spectral properties are then deduced. The applicability of CARS to practical temperature and concentration measurements in reactive media is then investigated. The experimental results obtained at ONERA using a conventional CARS equipment are presented. The second part of the chapter is devoted to the study of electronic resonance enhancement in CARS which shows great promise for sensitive detection of trace species, and for high resolution molecular spectroscopy. Some experimental results obtained on iodine vapor are finally presented.

A - CONVENTIONAL CARS

1 - CARS THEORY

In gases, CARS is observed when two collinear light beams with frequencies ω_1 and ω_2, called laser and Stokes respectively (with $\omega_1 > \omega_2$), traverse a sample with a Raman active vibrational mode of frequency $\omega_v = \omega_1 - \omega_2$. A new wave is then generated at the anti-Stokes frequency $\omega_3 = \omega_1 + \omega_1 - \omega_2 = 2\omega_1 - \omega_2$, in the forward direction and collinear with the pump beams (Fig. 16). This new wave results from the inelastic scattering of the wave at ω_1 by the molecular vibrations which are coherently driven by the waves at ω_1 and ω_2 (hence the name of the effect). We note that the same mechanism creates, for reasons of symmetry, a similar wave at $2\omega_2 - \omega_1$ (CSRS for coherent Stokes Raman scattering).

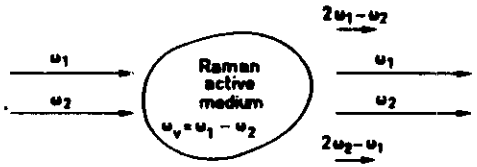

Fig. 16 - CARS and CSRS.

CARS is a nonlinear optical process. We recall that, in nonlinear optics, when intense optical beams are applied to the medium :

1 - a nonlinear polarization is created at the incident wave frequencies as well as at linear combinations of these frequencies,

2 - the coupling between this nonlinear polarization and the incident electric fields results in the amplification or attenuation of these fields, and in the growth of new electromagnetic waves as in the CARS process. The spatial and temporal evolution of these waves are described by the well-known Maxwell equations.

1.1 - The nonlinear polarization

At high field strengths, the polarization which is created in the medium can be expressed in terms of a power series in the field amplitudes :

$$\underline{\mathcal{P}} = \underline{\underline{\chi}}^{(1)}\,\underline{E} + \underline{\underline{\chi}}^{(2)}\,\underline{E}^{2} + \underline{\underline{\chi}}^{(3)}\,\underline{E}^{3} + \cdots \qquad (20)$$

where $\chi^{(m)}$ is the susceptibility tensor of order (m),
$\underline{\mathcal{P}}$ the polarization vector,
and $\underline{E}$ the electric field vector.

$\chi^{(1)}$ is the ordinary linear susceptibility of the medium and therefore $\chi^{(1)}$ is associated with linear effects such as dispersion and absorption. The quantities $\chi^{(2)}$ and $\chi^{(3)}$ are called the second and third order nonlinear susceptibilities of the medium ; $\chi^{(2)}$ is responsible for such effects as frequency doubling or parametric conversion, and vanishes in media possessing inversion symmetry, e.g. controsymmetric crystals, gases and liquids ; $\chi^{(3)}$ stands for a large class of effects such as third-harmonic generation and three-wave mixing via two photon and Raman nonlinearities [66]. Thus, CARS is only one of the many phenomena which arise from this cubic polarization.

Two methods can be used to derive the expression of this polarization : the first one uses a classical model to describe the fields interaction ; however, a more rigorous expression is obtained through a quantum mechanical calculation of the third-order susceptibility $\chi^{(3)}$.

a - the classical approach to polarizability

In this calculation, the molecular polarizability α is developed to first order as a function of the normal coordinate of vibration q, as expressed in Eq. (10). In the linear interaction of the waves with matter, the macroscopic polarization is given by :

$$\underline{\mathcal{P}} = N\alpha\,\underline{E} \qquad (21)$$

where the electric field is expressed by the sum :

$$\underline{E} = \frac{1}{2}\left(\underline{E}(z,\omega_1)\, e^{-i(\omega_1 t - k_1 z)} + \underline{E}(z,\omega_2)\, e^{-i(\omega_2 t - k_2 z)} + \text{c.c} \right) \qquad (22)$$

of the two incident fields travelling in the forward direction, along the Z axis ; $\underline{k}_1$ and $\underline{k}_2$ are their wave vectors. The vibration is driven in resonance by the force :

$$F = -\frac{\delta W}{\delta q}$$

where the energy of the system is :

$$W = -\frac{1}{2}\alpha \underline{E}^{2}$$

and where only the cross term $\underline{E}(z, \omega_1)\underline{E}^*(z, \omega_2)e^{-i[(\omega_1 - \omega_2)t - (\underline{k}_1 - \underline{k}_2)z]}$ is considered. The vibration is described by the damped harmonic oscillator equation :

$$\left(\frac{\delta^2}{\delta t^2} + \Gamma \frac{\delta}{\delta t} + \omega_v \right) q = \frac{F}{m} \qquad (23)$$

where Γ is the damping constant and m the reduced mass.

The solution of this equation is given by :

$$q = \frac{1}{4m} \frac{\delta \alpha}{\delta q} \frac{\underline{E}(z,\omega_1)\underline{E}^*(z,\omega_2)e^{-i[(\omega_1 - \omega_2)t - (\underline{k}_1 - \underline{k}_2)z]}}{D} + c.c \qquad (24)$$

$$\text{with } D = \omega_v^2 - (\omega_1 - \omega_2)^2 - i(\omega_1 - \omega_2)\Gamma \qquad (25)$$

Therefore, substituting Eqs. (10) and (24) into Eq. (21), the polarization component of frequency $\omega_3 = 2\omega_1 - \omega_2$ is given by :

$$\underline{\mathcal{P}}(z,t,\omega_3) = \frac{1}{2}\left(\underline{\underline{\chi}}^{(3)} \underline{E}^2(z,\omega_1)\underline{E}^*(z,\omega_2)e^{-i(\omega_3 t - \underline{k}_3' z)} + c.c \right) \qquad (26)$$

$$\text{with } \underline{k}_3' = 2\underline{k}_1 - \underline{k}_2 \quad \text{and} \quad \underline{\underline{\chi}}^{(3)} = \frac{N}{4m}\left(\frac{\delta \alpha}{\delta q}\right)^2 \frac{1}{D}$$

Here, the nonlinearity in the molecular polarizability is represented by the third-order nonlinear susceptibility $\underline{\underline{\chi}}^{(3)}$. The electromagnetic wave at the anti-Stokes frequency ω_3 can be written :

$$\underline{E}(z,t,\omega_3) = \frac{1}{2}\left(\underline{E}(z,\omega_3)e^{-i(\omega_3 t - \underline{k}_3 z)} + c.c \right) \qquad (27)$$

where $\underline{k}_3$ is the wave vector of the anti-Stokes wave, along the z axis.

The propagation of this wave is governed by the wave equation :

$$\left(\nabla - \frac{n^2}{c^2}\frac{\delta^2}{\delta t^2} \right) \underline{E}(z,t,\omega_3) = \frac{4\pi}{c^2} \frac{\delta^2}{\delta t^2} \underline{\mathcal{P}}(z,t,\omega_3)$$

The wave equation then can be reduced to the steady state equation :

$$\frac{\delta}{\delta z}\underline{E}(z,\omega_3) = \frac{i\pi\omega_3}{2c} \underline{\underline{\chi}}^{(3)} \underline{E}^2(z,\omega_1)\underline{E}^*(z,\omega_2)e^{i\delta k z} \qquad (28)$$

The growth condition for this wave, also called the phase-matching condition, is thus :

$$\delta k = \underline{k}_3' - \underline{k}_3 \simeq 0$$

b - quantum mechanical approach

More properly, the third-order polarization can be written under steady state conditions :

$$\underline{\mathcal{P}}^{(3)}(z,t,\omega_3) = \frac{1}{2}\left(\underline{P}^{(3)}(z,\omega_3)e^{-i(\omega_3 t - \underline{k}_3' z)} + c.c \right) \qquad (29)$$

with

$$\underline{P}^{(3)}(z,\omega_3) = \frac{1}{4} \underline{\underline{\chi}}^{(3)}(-\omega_3, \omega_1, \omega_1, -\omega_2)\underline{E}^2(z,\omega_1)\underline{E}^*(z,\omega_2) \qquad (30)$$

This equation (as Eq. (26)) gives the nonlinear relation between the incident electric fields and the polarization which is set up in the medium.

The quantum mechanical derivation of the nonlinear susceptibility terms is done through a perturbative treatment of the electric field interactions [95-97]. In the density operator formalism, the quantum state of the scattering molecules is represented, at point z, by the density operator ρ with the equation of motion :

$$\frac{\delta \rho^{(m)}}{\delta t}(z,t) = -\frac{i}{\hbar}\left(\left[H_0, \rho^{(m)}(z,t) \right] + \left[V(z,t), \rho^{(m-1)}(z,t) \right] \right) + \left. \frac{\delta \rho^{(m)}(z,t)}{\delta t} \right|_{damp} \qquad (31)$$

where $\rho^{(m)}$ is the density operator of order (m). H_0 is the free molecule Hamiltonian with discrete spectrum of eigenstates $|n\rangle$ corresponding to eigenvalues $\hbar\omega_n$; the perturbation Hamiltonian which describes the interaction of the molecules with the radiation field is $V(z, t) = -\underline{P} \cdot \underline{E}(z, t)$ in the dipolar approximation, $\underline{P}$ is the dipole moment operator; $\left.\frac{\delta \rho}{\delta t}\right|_{damp}$ is the damping term, which is determined by stochastic processes such as spontaneous emission of light and collisions between molecules. In the usual procedure, Eq. (31) is solved in an iterative mode, up to order 3, in order to get the third-order susceptibility $\underline{\underline{\chi}}^{(3)}$. Nevertheless, it has been shown by several authors [98, 99] that the susceptibility terms can also be obtained in a much shorter and easier manner, by means of a diagrammatic representation of the density operator.

The density operator at any specified interaction order can be shown to result from a number of contributions. Each of these contributions is associated with a specific time sequence of perturbations to the density operator. It has been shown that elementary time-ordered contributions can be visualized by a diagram [98]. The density operator formalism, in association with such a diagrammatic representation, leads to a rapid derivation of all relevant susceptibility terms [95-99], and

to an easy interpretation of the physical mechanisms involved [95-100]. This derivation will not be given here. However, the calculation shows that, if we use a set of four molecular levels $|a\rangle$, $|b\rangle$, $|n\rangle$, $|n'\rangle$ as depicted in the energy level diagram of Fig. 17, the CARS susceptibility can be written :

$$\underline{\underline{\chi}}^{(3)}(-\omega_3, \omega_1, \omega_1, -\omega_2) = \underline{\underline{\chi}}_R^{a,b,n,n'} + \underline{\underline{\chi}}_{N.R} \qquad (32)$$

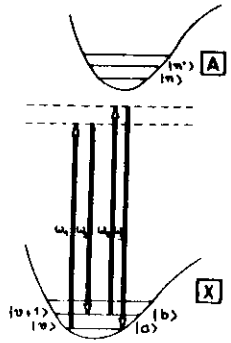

Fig. 17 - Energy level diagram of the CARS process.

where $\chi_R^{a,b,n,n'}$ is the Raman-resonant part associated with the Raman active transition of frequency ω_{ba} between $|a\rangle$ and $|b\rangle$, for the set of two excited electronic states $|n\rangle$ and $|n'\rangle$. In gas mixtures, part $\chi_{N.R.}$, which is called non resonant, is small and is contributed both by the probed molecules (to a small extent) and for the most part by the molecular species which do not possess a vibrational resonance near $\omega_{ba} = \omega_1 - \omega_2$. These molecular species are also called non-Raman-resonant (diluent molecules). $\underline{\underline{\chi}}_{NR}$ is composed of terms analogous to those of $\chi_R^{a,b,n,n'}$ but with nonresonant two-photon sum or difference denominators in place of the Raman resonance denominator. In the usual case where the number density N of the probed molecules is small compared to that of the diluent molecules, $\underline{\underline{\chi}}_{NR}$ is mainly contributed by the latter, and is therefore a frequency-independent real tensor (provided that there are no one- or two-photon electronic resonances in the diluent molecules).

The expression of the Raman resonant susceptibility is obtained by solving Eq. (31), [96] :

$$\chi_R^{a,b,n,n'} = \frac{N}{\hbar^3} \frac{1}{\omega_{ba} - \omega_1 + \omega_2 - i\Gamma_{ba}} (A+B)\left[\rho_{aa}^{\circ}(\alpha+\beta) - \rho_{bb}^{\circ}(\gamma+\delta)\right] \qquad (33)$$

with

$$A = \mu_{an'} \mu_{n'b} (\omega_{n'a} - \omega_3 - i\Gamma_{n'a})^{-1}$$

$$B = \mu_{an'} \mu_{n'b} (\omega_{n'b} + \omega_3 + i\Gamma_{n'b})^{-1}$$

$$\alpha = \mu_{bn} \mu_{na} (\omega_{na} + \omega_2 - i\Gamma_{na})^{-1}$$

$$\beta = \mu_{bn} \mu_{na} (\omega_{na} - \omega_1 - i\Gamma_{na})^{-1}$$

$$\gamma = \mu_{bn} \mu_{na} (\omega_{nb} - \omega_2 + i\Gamma_{nb})^{-1}$$

$$\delta = \mu_{bn} \mu_{na} (\omega_{nb} + \omega_1 + i\Gamma_{nb})^{-1}$$

N is here the number density of active molecules. The absorption frequencies from states $|a\rangle$ and $|b\rangle$ to state $|n\rangle$ are ω_{na} and ω_{nb} respectively, and the Γ's are the corresponding damping factors ; μ_{an} is the matrix component of the dipole moment operator $\underline{\mu}$, $\mu_{an} = \langle a | \underline{\mu} \cdot \hat{e}_1 | n \rangle$ where $\hat{e}_1$ is the unit vector in the direction of polarization of the ω_1 field ; μ_{bn}, $\mu_{n'b}$, μ_{an}, involve interactions with ω_2, ω_1 and ω_3 fields respectively.

The spectral dependence of the nonlinear optical susceptibility tensor $\underline{\underline{\chi}}^{(3)}(-\omega_3, \omega_1, \omega_1, -\omega_2)$ as a function of the applied field frequencies ω_1, ω_2, is directly reflected in the rate of growth of the signal wave at ω_3. By tuning the applied field frequencies and monitoring the resultant changes in the signal amplitude, one performs an analysis of the spectral properties of $\underline{\underline{\chi}}^{(3)}(-\omega_3, \omega_1, \omega_1, -\omega_2)$ and thus a nonlinear optical spectroscopy of the medium. As shown in Eq. (32), $\underline{\underline{\chi}}^{(3)}$ contains two parts : a Raman resonant χ_R and a non resonant $\underline{\underline{\chi}}_{N.R.}$. It is the presence of this nonresonant part which is one of the most severe problems in the application of CARS spectroscopy.

Off electronic resonance, all the coefficients A, B, α, β, γ, δ are of similar magnitude and the Raman resonant part (Eq. (33)) of the susceptibility thus reduces to :

$$\chi_R = \frac{N c}{\hbar \omega_1 \omega_2^3} (\rho_{aa}^{\circ} - \rho_{bb}^{\circ}) \frac{d\sigma}{d\Omega} \frac{1}{\omega_{ba} - \omega_1 + \omega_2 - i\Gamma_{ba}} \qquad (34)$$

where $\frac{d\sigma}{d\Omega}$ is the spontaneous Raman scattering cross-section defined in chapter III and $N\rho_{ii}^{\circ}$ is the population of unperturbed molecular state $|i\rangle$. A spectral analysis reveals the Raman resonances $[\omega_1 - \omega_2 = \omega_{ba}]$ contained in the denominator of Eq. (34) (also present in Eq. (25)). Thus, CARS spectroscopy, when carried out in the proper frequency domain, gives information about the Raman active vibrational modes of the medium. Identification of these vibrational resonances and measurement of their amplitudes are the basis for a whole line of experiments ranging from pure Raman spectroscopy to analytical chemistry.

1.2 - The CARS signal intensity

The anti-Stokes wave travelling in the forward direction, along the z axis, is a solution of the wave equation. Integrating Eq. (28), we obtain the field amplitude $\underline{E}(z, \omega_3)$ and then, according to the following expression :

$$I_n = \frac{c}{8\pi} |\underline{E}(z, \omega_n)|^2 \qquad \text{with } n = 1, 2, 3 ,$$

we obtain the anti-Stokes intensity :

$$I_3 \propto \left| \underline{\underline{\chi}}^{(3)}(-\omega_3, \omega_1, \omega_1, -\omega_2) \hat{e}_3 \hat{e}_1 \hat{e}_2 \right|^2 I_1^2 I_2 \left(\frac{\sin \delta k z/2}{\delta k/2} \right)^2 \quad (35)$$

where $\hat{e}_1$ and $\hat{e}_2$ are the unit polarization vectors of the pump waves.

Two remarks can be drawn from Eqs. (28) and (35) :

1 - the anti-Stokes field polarization vector is oriented along the vector $\underline{\mathcal{E}}_3 = \underline{\chi}^{(3)}(-\omega_3, \omega_1, \omega_1, -\omega_2)\, \hat{e}_1\, \hat{e}_1\, \hat{e}_2$, which depends on the applied field polarizations as well as on the tensor properties of the susceptibility. This vector has two independent components associated with the nonresonant and the Raman resonant parts of the susceptibility (as shown in Eq. (32)). This property can be used for nonresonant background cancellation in the spectra.

2 - The CARS signal intensity, which is the parameter directly measured using photodetectors, is proportional to $|\mathcal{E}_3|^2$ (Eq. 35) and, therefore, to the squared number density of the medium. It also has a sinusoidal dependence on z ; in gases, however, we have $\delta k \simeq 0$ because the dispersion is weak, so that the behavior is parabolic over long distances. Pump depletion would eventually limit this parabolic growth.

2 - PRACTICAL APPLICATION OF CARS

The laws governing the signal growth and the spectral properties of CARS have been established in the preceding chapter. We shall see now that CARS offer many advantages over other optical methods for non intrusive spatially resolved diagnostics of gases and reactive media.

a - Spatial resolution

Unfocused parallel beams with large diameters are seldom used because no spatial resolution is possible in this geometry. Since the growth of the power density I_3 is proportional to $I_1^2 I_2$, it seems advantageous to focus the beams to a small diameter and to use high peak power sources. If the condition $\delta k = 0$ is assumed, then it can be shown that :

- the anti-Stokes flux is contained within the same cone angle as the pump beams emerging from the focal region,
- this flux is generated for the most part within the focal region (where $I_1^2 I_2$ is large),
- the total power in the anti-Stokes beam, some distance beyond the focus, is independent of beam diameter and focal length and is given by :

$$P_3 = \left(\frac{2}{\lambda}\right)^2 \left(\frac{4\pi^2 \omega_3}{c^2}\right)^2 |\mathcal{E}_3|^2 P_1^2 P_2$$

where refractive indices were taken as unity, $\lambda = 2\pi c/\omega$ with $\omega \simeq \omega_1 \simeq \omega_2 \simeq \omega_3$, and P_1 and P_2 are the powers at ω_1 and ω_2 respectively.

In practical experiments, the spatial resolution is on the order of 1 to 20 mm, with laser beams of good optical quality. A particular beam arrangement called BOXCARS has been proposed for better resolution [101].

b - Spectral information

The spectra are usually retrieved by holding ω_1 fixed, tuning ω_2 so that $\omega_1 - \omega_2$ is swept across the resonances of interest, while monitoring the anti-Stokes flux (Fig. 18a). A CARS spectrum can also be obtain in a single pulse by using a broadband arrangement, as shown in Fig. 18(b).

As in SRS, informations about the nature, temperature and concentration of the species involved are obtained from the spectra using Eq. (34) :

- Each molecular species has a particular set of vibrational normal modes which leads to unambiguous identification of the gas components.
- Line intensities can be used to monitor populations in distinct rovibronic levels and deduce the rotational and vibrational temperatures by calculating the Boltzmann coefficients

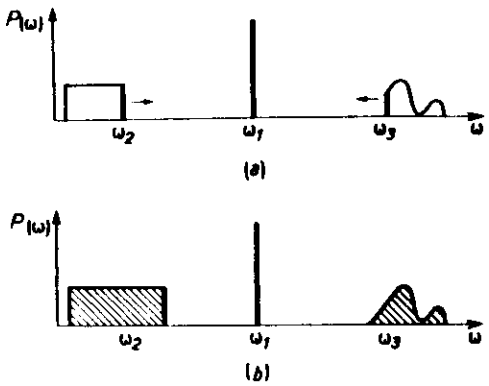

Fig. 18 - Retrieval of CARS spectra : a) scanning ; b) multiplex.

We note, however, that the existence of the nonresonant susceptibility poses a problem with the detection of trace species in mixtures, since the nonresonant contribution from the diluent gases may swamp the Raman-resonant part of the trace species of interest. As a matter of fact, detection sensitivities are in the range of 10^2 to 10^4 ppm for most cases of interest. These figures can be improved by a factor of about 30 if advantage is taken of the different tensor properties of X_{NR} and X_R (polarization CARS).

c - CARS instrumentation and results

The spectrometer is composed of a YAG laser coupled with a tunable dye laser ; it has been developed jointly with Quantel (Fig. 19). This system can operate in different modes, e.g. with :

- collinear beams for detection of traces species,
- BOXCARS to improve spatial resolution,
- polarization cancellation of nonresonant background,
- multiplex arrangement for single shot measurements.

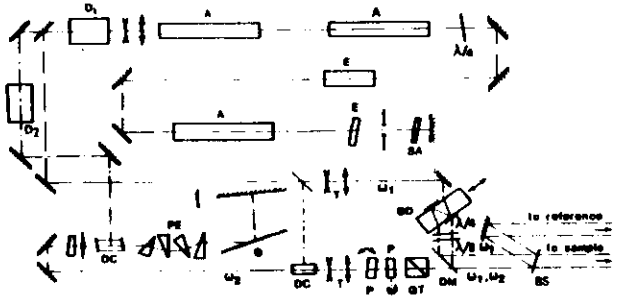

Fig. 19 - Laser source assembly. A : Nd yag amplifier. BD : parallel plate for production of parallel beams for boxcars (boxcars arrangement shown, translation of the plate allows passage to collinear arrangement without loss of alignment). BS : beam splitter for reference channel. D1, D2 : KDP doublers. DC : dye cell. DM : dichroic mirror. E : Fabry-Perrot etalon. G : grating. GT : Glan-Thompson prism. P : AR coated parallel plate for beam translation. PE : Prism expander. SA : saturable absorber. T : telescope. λ/4 and λ/2 are quarter-wave and half-wave plates respectively. ω_1 : "laser" beam. ω_2 : "stokes" beam.

The passively Q-switched Yag oscillator,with two amplifiers and one frequency doubler,delivers over 150 mJ of radiation at 532 nm in 10 ns pulses at 1 to 10 Hz (ω_1 beam). A part of the green radiation pumps the dye chain which is composed of a dye laser and one amplifier stage and produces the "Stokes" beam at ω_2. The linewidth is 0.7 cm^{-1} ; it can be easily reduced to 0.07 cm^{-1} for high resolution spectroscopy. The dye chain delivers from 1 to 5 mJ of tunable radiation in a diffraction-limited beam over the useful CARS range of 560-700 nm, regardless of the linewidth. A broadband mode of operation is also provided for the dye laser, giving about 50 cm^{-1} linewidth; this mode is used for multiplex CARS experiments, in conjunction with a spectrograph and an optical multichannel analyser [83]. The anti-Stokes signals are filtered by means of compact double monochromators preceded by dichroic filters ; detection is done with PM tubes. We use a reference cell filled with 50 bars of Argon which only has a nonresonant susceptibility. The CARS emission from this cell permits normalization of the signals generated in the sample, thus eliminating the influence of the laser power fluctuations. The photocurrent pulses from signal and reference channels are treated by an electronic device that gates them, calculates their ratio, square root and average for a fixed number of shots.

In some experiments, the technique of background suppression using the tensor properties of the nonlinear susceptibility leads to an improved detectivity. It has been studied in detail for collinear beams and several possible polarization arrangements have been described [83, 102]. In BOXCARS, some flexibility is afforded by the availability of two spatially distinct "laser" beams at ω_1, which can have different polarizations. A discussion of that problem will be found in reference [78].

The feasibility of concentration measurements in flames by CARS was shown in 1973 [70]. Since then, many experiments have been carried out and many species have been detected.

The first measurement of practical interest was conducted in 1978 at ONERA on a simulated turbomachine combustor fueled by kerosene [78]. Numerous spectra have been recorded. The spectrum of N_2 taken in that combustor on the flow centerline without background cancellation is presented in Fig. 20. In this spectrum, the first vibrational hot band is clearly seen. Numerical processing of this data yields a concentration of 78 ± 5 % and a temperature of 1150 ± 50 K, in good agree-

ment with gas chromatograph and thermocouple measurements giving 78 % and 1050 K respectively. Other gases studies were O_2, CO_2 (Fig. 21) and CF_4.

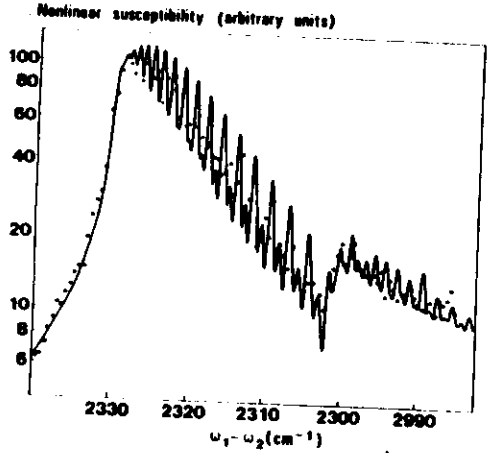

Fig. 20 - Time-averaged scanning CARS spectrum of N_2 in the exit plane of combustor ; 10 laser shots are averaged at each point.

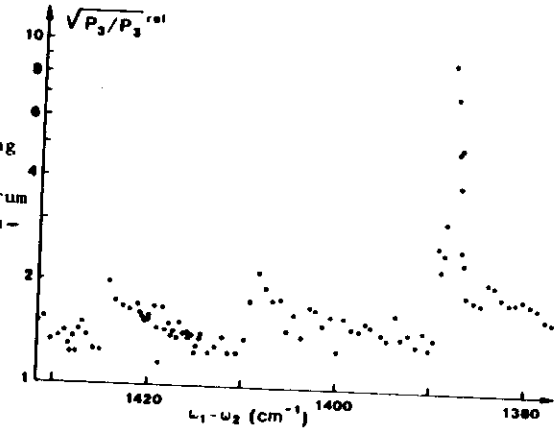

Fig. 21 - Time-averaged scanning CARS spectrum of CO_2 taken at the same location as the spectrum of figure 20 ;6 shots are averaged at each point.

A low pressure discharge in H_2 was investigated in order to gather information on the population distribution in the rovibrational manifold of the H_2 ground electronic state [82]. The plasma pressure was held at 1.3 10^{-4} bars. Typical results are shown in Figs. 22, 23.

Detection of H_2 in a premixed ethylene + air flame has been conducted for temperature and H_2 concentration measurements. BOXCARS with polarization cancellation was used. A flame investigation along the burner axis was carried out ; the results are shown in Fig. 24. The reader is referred to reference [78] for other results obtained with this instrument and to references [74] and [97] for reviews of other works in various experimental situations.

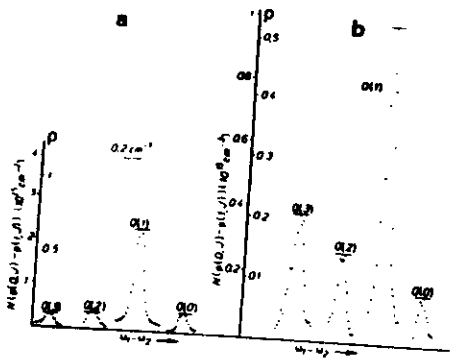

Fig. 22 - Rotationally resolved CARS Q branch of H_2. The fundamental Raman transition $[0, J] \rightarrow [1, J]$ is sounded (a) without the discharge, showing a rotational temperature T = 290 ± 5 K and (b) with a discharge of 90V, 3A ; we then measure T = 475 ± 15 K.

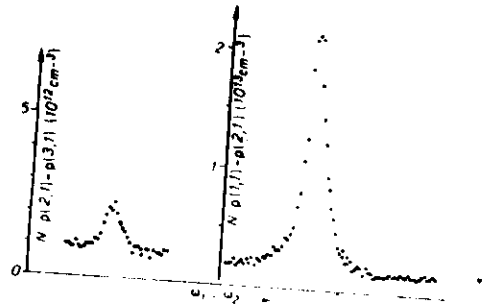

Fig. 23 - CARS fundamental Q line of H_2 from initial levels J = 1, V = 1 (right) and J = 1, V = 2 (left) in the discharge.

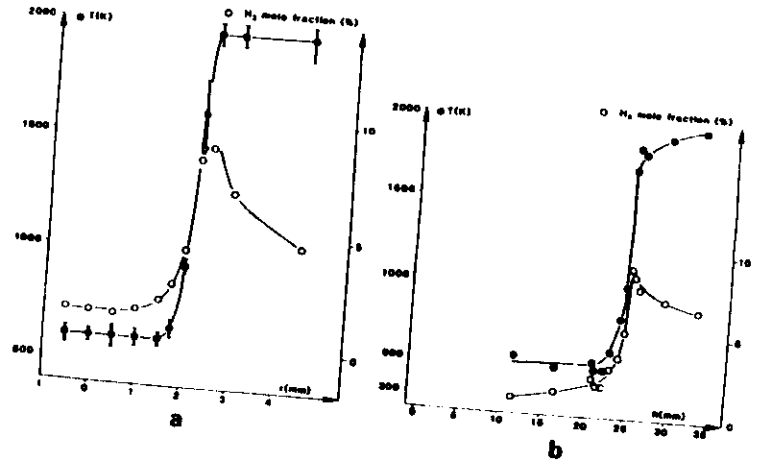

Fig. 24 - Radial (a) and vertical (b) profiles of H_2 concentration in the burner ; the radial measurements were taken 11.5 mm above the burner.

B - RESONANCE-ENHANCED CARS

We recall that the detectivity offered by CARS in the chemical analysis of mixtures is limited, due to the presence of the diluent background susceptibility. The detectivity can be improved by either cancelling the background or enhancing the Raman-resonant part relative to the background. The present discussion is devoted to the problem of electronic resonance enhancement of the CARS susceptibility. Resonant CARS spectra were first seen in solutions by Chabay et al [91]. The demonstration in the gas phase is more difficult, and was given somewhat later using the I_2 molecule [93] ; from these results, a detailed theory of the spectral properties was also proposed [96]. The improvement in detection sensitivity ranges from 10^2 to 10^4, depending on the wavelength used ; this certainly justifies continuation of this delicate work on other molecules and radicals which are of interest to combustion. Several observations in C_2 [103] and NO_2 [94, 104] were reported recently.

1 - SPECTRAL PROPERTIES

Resonance CARS spectroscopy is usually carried out by holding ω_1 fixed near a one-photon absorption and by tuning ω_2 (Fig. 25). The rules governing the interpretation of the resonance CARS spectra have been discussed some time ago [96, 97] and we shall only summarize the results here. The rules are deduced from the consideration of the susceptibility expression. When the electronic resonances are approached, only two terms in Eq. (32) become large, thus we have :

$$\chi_R \simeq \frac{N}{\hbar^3} \frac{1}{\omega_{ba} - \omega_1 + \omega_2 - i\Gamma_{ba}} (\rho^0_{aa} A\beta - \rho^0_{bb} A\gamma) \qquad (36)$$

Since A, β and γ all undergo large enhancements and large variations as the field frequencies are varied, the spectral analysis is complicated somewhat. The CARS spectrum may present a complex structure, very different from the off-resonance case, since any of the three frequencies ω_1, ω_2 and ω_3 may come into resonance with absorption lines. In addition, some other terms, which are not Raman-resonant and therefore, which are not included in Eq. (32), may become large [105]. However, simplifications occur since :

- when the Raman spectrum is analysed $\omega_1 - \omega_2$ is tuned over a finite spectral domain and a limited number of Raman transitions contribute to the susceptibility. For a given Raman transition between two particular rovibrational levels $|a\rangle$ and $|b\rangle$ of the ground electronic state (Fig. 25), there are only a few types of allowed one-photon transitions to the excited electronic state, e.g. $\Delta J = \pm 1$ for iodine. Therefore, the number of absorption lines that ω_2 and ω_3 can reach to enhance $\chi^{(3)}$ is finite ,
- one can often assume that $\rho^0_{bb} \ll \rho^0_{aa}$ in Boltzmann equilibrium and in the range of temperature used for the experiments. Then the term proportional to ρ^0_{bb} in Eq. (36) can be neglected.

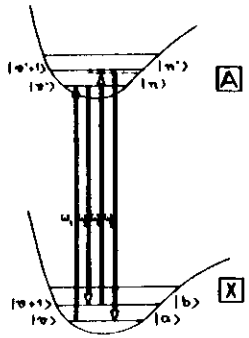

Fig. 25 - Energy level diagram of the resonance CARS process.

There are three types of lines associated with the initial rovibronic state $|a\rangle$ as depicted in Fig. 26. We call these laser-enhanced Raman resonances (Fig. 26(a)), double-electronic resonances (Fig. 26(b)) and anti-Stokes-enhanced Raman resonances (Fig. 26(c)). Both fundamental and overtone vibrational bands are possible when ω_2 is tuned to successive higher vibrational levels of the ground electronic state. The order of magnitude of resonance enhancement can change significantly from one overtone to the other, depending on the rotational structure of the absorption spectra of the molecular species investigated. Obviously, a preliminary knowledge of this fine structure is required to perform the assignments of the resonance CARS lines.

A noteworthy character of the double electronic resonances is that their positions in the spectrum, which are given by the condition $\omega_1 - \omega_2 = \omega_{n'a} - \omega_1$, are a function of ω_1, contrary to the Raman resonances for which ω_{ba} depends only on the spectroscopic constants of the molecule (Eq. 7).

The observation of double electronic resonances is of considerable importance to the spectroscopist, since one can easily identify the corresponding $\omega_{n'a}$ absorption lines if the ω_{na} transition, in resonance with ω_1, is known. This can facilitate the analysis of unknown portions of absorption spectra.

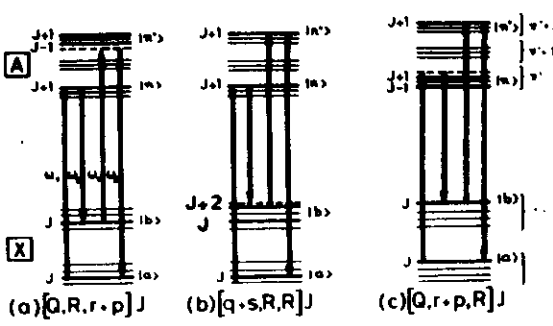

Fig. 26 - Energy level diagrams representing the states contributing to resonance-enhanced CARS in a diatomic molecule such as I_2.
(a) ω_{na} (laser) enhanced fundamental ($\Delta V=1$) Raman transition.
(b) double electronic resonance with $\omega_1 = \omega_{na}$ and $\omega_3 = \omega_{n'a}$.
(c) $\omega_{n'a}$ (anti-stokes) enhanced fundamental Raman transition.

2 - EXPERIMENTAL RESULTS

The resonance CARS spectrometer is composed of two flash-pumped dye lasers producing beams with divergence near the diffraction limit and peak power of 1 to 10 kW between 480 and 650 nm (Fig. 27). The linewidths are 0.02 cm^{-1} and 0.05 cm^{-1} for laser and Stokes frequencies respectively. Their beams are made collinear ; they are both horizontally polarized.

The experimental procedure used in iodine is detailed in reference [78]. The laser frequency is tuned to the R[v' = 13 - v = 1] 67 absorption line of the B ← X electronic transition,to achieve resonance enhancement. Then ω_2 is tuned to the v = 6 level of ground electronic state X in order to scan the fifth overtone Raman band [v' = 6 - v = 1].

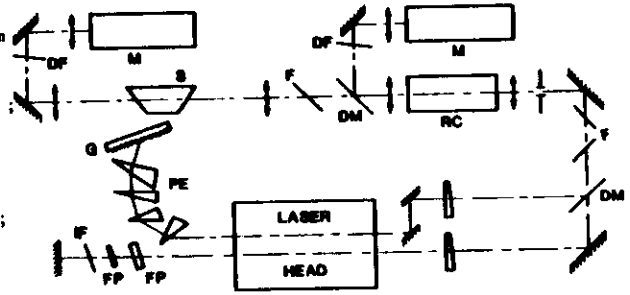

Fig. 27 - Schematic diagram of resonance CARS spectrometer. DF : dichroic filter ; DM : dichroic mirror ; F : colored filter ; FP : Fabry-Perrot etalon ; IF : interference filter ; G : grating ; M : monochromator and detector assembly ; PE : prism beam expander ; RC : reference cell ; S : sample cell.

For the spectra of Fig. 28, the temperature of iodine in the cell is held at 45°C,so that the partial pressure of I_2 is about 2.10^{-3} bar mixed with air at a total pressure of 1 bar. When ω_1 is slightly shifted about ω_{na}, the double electronic lines (dotted line of Fig. 28) move apart or to the Raman lines. This drift which is clearly visible from Fig. 28 (a) to 28 (d),facilitates the assignment of the lines. The

latter is given in table II. The notation used to label these resonances is that of ref. [93] : the first letter in the bracket defines the Raman transition ω_{ba}, the second and the third ones are the ω_{na} and $\omega_{n'a}$ transition respectively. Upper case lettering is used for exact or near exact resonance with the field frequencies, lower case lettering otherwise. For example, the resonance depicted in Fig. 26 (a) is labeled : $[q(v+1-v), R(v'-v), r \text{ or } p\ (v'+1-v)]J$.

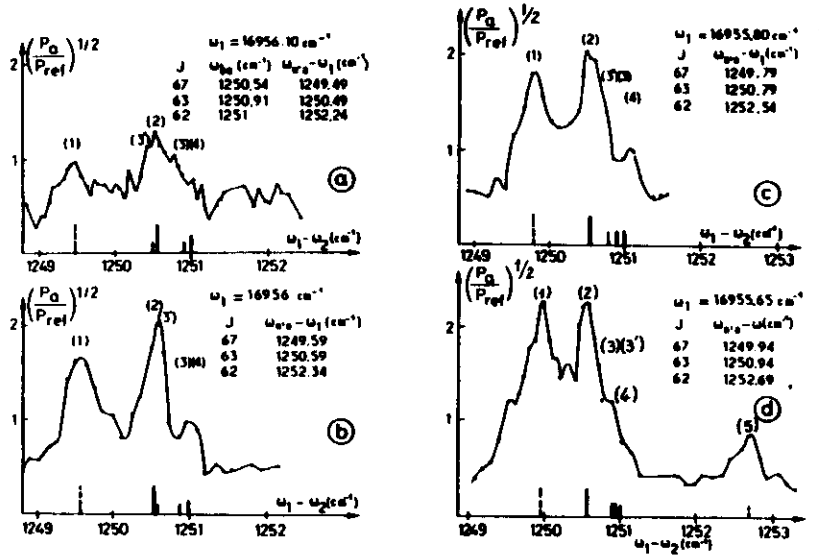

Fig. 28 - Spectrum of I_2 at 45°C (1.9 mb) in air. The spectral position and estimated relative intensities of the resonance CARS lines are indicated on the horizontal axis (using Eq. (36)). The positions of the Raman lines have been calculated using spectroscopic constants of ref. [106] The positions of the electronic lines have been calculated using the positions of the absorption lines given in ref. [107] All these values are listed in the inset table.

TABLE II - RESONANCE CARS LINE ASSIGNMENTS

(1)	[q(6 - 1), P(13 - 1), R(27 - 1)] 67
(2)	[Q(6 - 1), R(13 - 1), r(27 - 1)] 67
(3)	[Q(6 - 1), P(13 - 1), P(27 - 1)] 63
(3')	[q(6 - 1), P(13 - 1), P(27 - 1)] 63
(4)	[Q(6 - 1), P(13 - 1), p(27 - 1)] 62
(5)	[q(6 - 1), P(13 - 1), P(27 - 1)] 62

We observe equal intensities for Raman and double electronic lines pertaining to the same J level. This reflects the fact that both lines have the same width ; the dominant broadening mechanism at STP is collisional broadening. Therefore, all the linewidths are equal in Eq. (36). As the buffer gas pressure decreases, the narrowing of the Raman and absorption lines results in a growth of the CARS signal,until the Doppler limit is reached. This growth clearly appears in Fig. 29 for which the air pressure was reduced to 10^{-2} bar. The line intensities are increased by one order of magnitude as expected from the crude calculation of resonant susceptibility (using Eq. (36)) which is given in table III. However, as the Raman and absorption lines do not have the same widths [95], there is an intermediate pressure domain (between 8.10^{-3} and 5.10^{-4} bar for I_2) in which Doppler and collisional broadenings are mixed. Beyond 8.10^{-3} bars of total pressure, the one-photon electronic transitions, which have been so far collision broadened, become Doppler broadened ; their Doppler widths are about 0.015 cm^{-1} for I_2. The Raman transitions are still collision-broadened with a width of about 0.004 cm^{-1} [table IV]. Figure 30 displays the change in intensity ratio between Raman and electronic lines. The ratio of corresponding Raman and double electronic lines is close to 2 which is in good agreement with the calculated value for a total pressure of about 2.10^{-3} bar.

$$\frac{I_{3_{Ram.}}}{I_{3_{Elect.}}} \propto \sqrt{\frac{\chi^{(3)}_{Ram}}{\chi^{(3)}_{Elect.}}} \propto \sqrt{\frac{\Gamma_{elect.}}{\Gamma_{Ram.}}} = \sqrt{3,75}$$

ω_1 (cm^{-1})	16 955.65	16 955.90	16 955.74	
Total pressure (bar) / Iodine temperature (°C)	1	$1.5\ 10^{-2}$	5.10^{-3}	2.10^{-3}
31	0.6	6	38.6	86.9
45	2.3	23.2	148.2	333.3

TABLE III - The resonant susceptibility (arbitrary unit) is given as a function of total pressure. This estimation is done using Eq. (36) and for the Raman line [Q(6 - 1), R(13 - 1), P(27 - 1)] 67.

Attention should be paid to the laser wavelength stability in these experiments. Close to resonance, a very small drift of the frequency ω_1 results in a quite significant change of the line intensities as seen in Fig. 30 (b) and 30 (c).

PRESSURE (bar) / CARS LINE	1	2.10^{-2}	2.10^{-3}	5.10^{-4}
RAMAN	0.2	0.04	0.004	0.001
DOUBLE-ELECTRONIC	0.2	0.04	0.015	0.015

TABLE IV - Resonance CARS linewidth (cm^{-1}) in I_2 as a function of total pressure.

Finally, regarding the application to trace species detection, we note that these lines are about 100 times stronger than atmospheric O_2 vibrational lines, although the number density in the respective rotational sublevel $|a\rangle$ is about 2000 times smaller in I_2 than in O_2 . We therefore estimate that practical detectivities in flames at atmospheric pressure for resonance enhanced CARS should be in the range of 0.1 to 10 ppm.

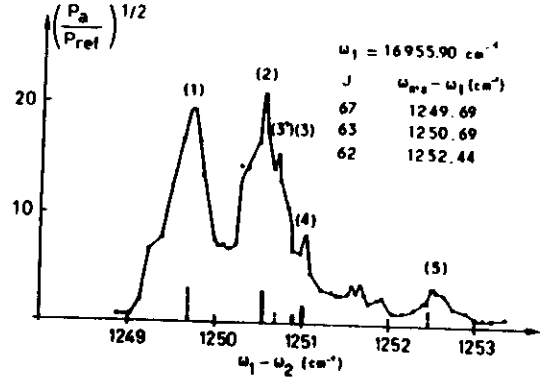

Fig. 29 - Spectrum of I_2 at 45°C in 10^{-2} bar of air.

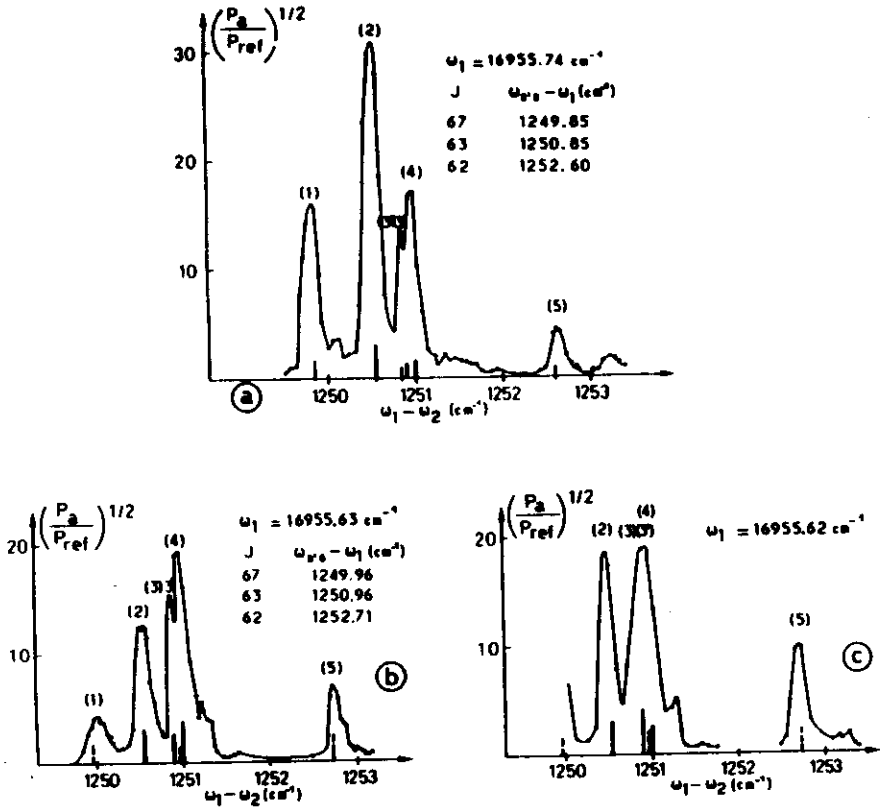

Fig. 30 - Spectrum of I_2 at 33°C (0.7 mb) in 2.10^{-3} bar of air.

CONCLUSION

We have reviewed some of the most important optical techniques for diagnostics, which can all provide non intrusive and specific temperature and concentration measurements in reactive media. These techniques have been very actively studied because of their advantage over the widely used conventional techniques which require the insertion of solid probes.

It is worthwhile to summarize their relative advantages and drawbacks, and to indicate what applications they are particularly well suited for.

The fluorescence technique, which offers very strong signal strength, seems a very attractive method for trace species analysis. However, because of quenching, the informations which are obtained from fluorescence spectra are difficult to interpret. We note that the problem of quenching can be partly resolved by using saturated LIF.

The low scattering cross-section of the SRS is the major drawback of this technique. However, when the concentration of major constituents is to be measured, it is preferable to use Raman scattering as a precise and reliable probe of gas system. For trace species, fluorescence is the preferred technique but then concentration measurements are less accurate. Improvement in the collector optics and data acquisition equipment, including the photomultiplier performance, may lead to higher signal to noise ratios. For example, partial pressure as low as 10^{-5} atm. are detectable by SRS in mixtures when there is no interference from sources of noise like stray light.

The unique properties of CARS, namely large signal strength collimated beam, and absence of fluorescence interference, make this technique capable of discriminating more easily than SRS against numerous sources of noise. However, the CARS detectivity is limited by the nonresonant background of diluent species. At this point, it must be emphasized that SRS and CARS detectivities are not directly comparable since the SRS detectivity depends on the total number of molecules of interest and is expressed in terms of a partial pressure, whereas the CARS sensitivity is given in terms of a mixing ratio due to the presence of the diluent background. The detectivity then is of the order of 0.1 to 1 %. By using

background cancellation, the detection sensitivity is lowered to 10 to 1000 ppm for usual gases in flames. Thus, CARS is now the best technique for non intrusive flame diagnostics and has reached the stage of being used by combustion engineers for practical measurements. However, the equipment for CARS is complicated, delicate and more expensive than for SRS.

Finally resonance CARS appears as a very attractive development since the large enhancement observed [78] leads to an improved sensitivity. Application of resonance-enhanced CARS to the detection of radical species in reactive media is very promising. For example, we are now working on the measurement of concentrations of molecular radicals such as C_2 and CH, which appear as a result of hydrocarbon decomposition in flames ; these measurements will provide direct informations about soot formation and the kinetics of chemical reactions.

BIBLIOGRAPHY

[1] - H.C. Van de Hulst, Light scattering by small particles, John Wiley, New York (1957).

[2] - R. P. Bauman, Absorption Spectroscopy, John Wiley, New York (1962).

[3] - K. Fujiwara, N. Omenetto, J.B. Bradshaw, J. N. Bower, S. Nikdel and J.D. Winefordner, Spectrochim. Acta., 34B, 317 (1979).

[4] - M.B. Blackburn, J.M. Mermet and J.D. Winefordner, Spectrochim. Acta, 34A, 847 (1978).

[5] - J.W. Daily, Appl. Opt., 17, 1610 (1978).

[6] - W. Demtröder, in : Analytical Laser Spectroscopy (Edited by N. Omenetto), chapter 5.,Wiley, New York (1979).

[7] - D.R. Crosley (editor), Laser probes for combustion chemistry, American Chemical Society symposium series, vol. n° 134, Washington, D.C.(1980).

[8] - C.M. Sadowsky and J.E.H. Vanoverschelde, The measurement of mass density in a turbulent wake by means of Rayleigh scattering from a laser beam, TN 1764/67, Canadian Armament Research and Development Establishment (CARDE), Quebec, Canada.

[9] - G. Placzek, Rayleigh strenung and Raman effect, Hand. Radiol. Akademische Verlagegesellshaft VI (1934).

[10] - M. Lapp, C.M. Penney and J.A. Asher, Application of light scattering techniques for measurements of density, temperature and velocity in gas dynamics, ARL 73-0045 (April 1973).

[11] - D.A. Leonard, Development of a laser Raman aircraft turbine engine exhaust emissions measurement system, AVCO Everett Res., Note 914 (1972).

[12] - H.A. Szymanski (Editor), Raman Spectroscopy Theory and Practice, Plenum Press (1967).

[13] - A. Anderson (editor), The Raman effect, Bekker, New York (1971).

[14] - B.P. Stoicheff, High Resolution Raman spectroscopy, Adv. Spectroscopy., I, pp 91-174, Interscience (1959).

[15] - P.P. Shorigin, Dokl. Akad. Nauk., SSSR, 87, 201 (1952).

[16] - R.E. Begley, A.B. Harvey and R.L. Byer, Appl. Phys. Lett., 25, 387 (1974).

[17] - P.R. Regnier, F. Moya and J.P.E. Taran, AIAA Paper n° 73-702 (July 1973).

[18] - R. Bailly, M. Péalat and J.P.E. Taran, à paraître.

R. Bailly, M. Péalat and J.P.E. Taran, Etudes aérodynamiques par diffusion Raman et par fluorescence, Document interne ONERA, 1976.

[19] - A.P. Baronavski and J.R. Mac. Donald, J. Chem. Phys., 66, 3300 (1977).

[20] - A.P. Baronavski and J.R. Mac. Donald, Appl. Opt., 16, 1897 (1977).

[21] - C.C. Wang and L.I. Davis JR., Appl. Phys. Lett., 25, 34 (1974).

[22] - R.H. Barnes, C.E. Moller, J.F. Kircher and C.M. Verber, Appl. Opt., 12, 2531 (1973).

[23] - S.V. Filseth, H. Zacharias, J. Danon, R. Wallenstein and K.H. Welge, Chem. Phys. Lett., 58, 140 (1978).

[24] - D.G. Jones and J.C. Mackie, Combustion Flame, 27, 143 (1976).

[25] - S.J. Weeks, H. Haraguchi and J.D. Winefordner, Anal. Chem., 50, 360 (1978).
J.D. Winefordner, New Applications of lasers to chemistry, p. 50, ACS Symposium Series n° 85 (1978).

[26] - Laser Raman Gas Diagnostics, Proceeding of the Project SQUID, Laser Raman Workshop of the measurement of gas properties, May 10-11, 1973, Schenectady, edited by M. Lapp and C.M. Penney, Plenum Press, New York, London (1974).
M. Lapp and C.M. Penney (editors), Laser Raman gas diagnostics, Plenum Press, New York, London (1974).

[27] - Proceedings of project SQUID, Workshop on combustion measurements in jet propulsion systems, edited by R. Goulard, Purdue University, Lafayette, Indiana (1975).

[28] - Experimental diagnostics in gas phase combustion systems, Progress in Astronautics and Aeronautics, Vol. 53, Edited by B.T. Zinn, Martin Summerfield Series Editor (1977).

[29] - R. Goulard, J. Quant. Spectrosc. Radiat. Transfer, 14, 969-974 (1974).

[30] - S. Lederman, Modern diagnostics of combustion, AIAA Paper n° 76-26, 14th Aerospace Sciences Meeting, Washington, D.C., 26-28 January 1976.

[31] - R.E. Setchell, Time-averaged measurements in turbulent flames using Raman spectroscopy, AIAA Paper n° 76-28, 14th Aerospace Sciences Meeting, Washington D.C., 26-28 January, 1976.

[32] - D.A. Leonard, Field tests of a laser Raman measurement system for aircraft engine exhaust emissions, AVCO Everett Research Laboratory Inc., Report AFAPL-TR 74-100 (October 1974).

[33] - R. Bailly, M. Péalat and J.P.E. Taran, Opt. Commun., 17, 68 (1976).

[34] - R.W. Terhune, Bull. Amer. Phys. Soc., 8, 359 (1963).

[35] - P.D. Maker and R.W. Terhune, Phys. Rev., 137, A801 (1965).

[36] - C.H. Muller, III, K. Schofield and M. Steinberg in : Laser probes for combustion chemistry (ed. by D.R. Crosley), Am. Chem. Soc. Symp. series, vol. 134, Washington, D.C., 1980, p. 103.

[37] - J.H. Bechtel and R.E. Teets, Appl. Opt., 18, 4138 (1979).
J.H. Bechtel, Appl. Opt., 18, 2100 (1979).
J.H. Bechtel in : Laser probes for combustion chemistry (ed. by D.R. Crosley), Am. Chem. Soc. Symp. series, vol. 134, Washington, D.C., 1980, p. 85.

[38] - M.J. Cottereau and D. Stepowski in : Laser probes for combustion chemistry (ed. by D.R. Crosley), Am. Chem. Soc. Symp. series, vol. 134, Washington, D.C., 1980, p. 131.
D. Stepowski and M.J. Cottereau, Appl. Opt., 18, 354 (1979).

[39] - D.R. Grieser and R.H. Barnes in : Laser probes for combustion chemistry (ed. by D.R. Crosley), Am. Chem. Soc. Symp. series, vol. 134, Washington, D.C., 1980, p. 153.

[40] - D.S. Coe and J.I. Steinfeld in : Laser probes for combustion Chemistry (ed. by D.R. Crosley), Am. Chem. Soc. Symp. series, vol. 134, Washington, D.C., 1980, p. 159.

[41] - E.H. Piepmeier, Spectrochim. Acta., 27B, 431 (1972).

[42] - J.W. Daily, Appl. Opt., 15, 955 (1976).

[43] - J.W. Daily, Appl. Opt., 16, 568 (1977).

[44] - N. Omenetto and J.D. Winefordner, Progr. Anal. Atomic Spectrosc., 2, (12), 1 (1979).

[45] - P.A. Bouczyk and J.A. Shirley, Combustion flame, 34, 253 (1979).

[46] - A.C. Eckbreth, P.A. Bouczyk and J.A. Shirley, Investigation of saturated laser fluorescence and CARS spectroscopic techniques for combustion diagnostics, U.S., EPA Report n° 600, 7-78-104 (1978).

[47] - M. Aldén, H. Edner, S. Svanberg and T. Högberg, Combustion studies with laser techniques, Göteborg Institute of Physics Reports, GIPR-206, March 1980.

[48] - R.P. Lucht and N.M. Laurendeau, Appl. Opt., 18, 856 (1979).

[49] - A.I. Kotlar, A. Gelb and D.R. Crosley in : Laser probes for combustion chemistry (ed. by D.R. Crosley), Am. Chem. Soc. Symp. series, vol. 134, Washington, D.C., 1980, p. 137.

[50] - R.P. Lucht, D.W. Sweeney and N.M. Laurendeau in : Laser probes for combustion chemistry (ed. by D.R. Crosley), Am. Chem. Soc. Symp. Series, vol. 134, Washington, D.C., 1980, p. 145.

[51] - G. Herzberg, Spectra of Diatomic Molecules, Van Nostrand, New York (1963).

[52] - J.W. Nibler, J.R. Mc. Donald and A.B. Harvey, Opt. Commun., 18, 3 (1976).

[53] - L.A. Arguello, G.F. Mendes and R.C.C. Leite, Appl. Opt., 13, 1731 (1974).

[54] - A.C. Eckbreth, AIAA Paper n° 76-27, January 1976; Laser Raman Combustor Thermometry, Paper 3C-1245 presented at the Fifth International Conference on Laser Spectroscopy, Universität Freiburg, 2-8 Septembre 1976, Edited by E.D. Schmidt, J. Brandmüller, W. Kiefer, B. Schrader and H.W. Schrötter.

[55] - M. Drake, M. Lapp, C.M. Penney and S. Warshaw, Measurements of temperature and concentration fluctuations in turbulent diffusion flames using pulsed Raman spectroscopy, to appear in Proceedings of the 19th International Symposium on Combustion.

[56] - S. Warshaw, M. Lapp, C.M. Penney and M. Drake, Temperature-velocity correlation measurement for turbulent diffusion flames from vibrational Raman scattering data, in : Laser Probes for combustion Chemistry (Ed. by D.R. Crosley), Am. Chem. Soc. Symp. Series, vol. 134, Washington, D.C., 1980.

[57] - M. Lapp, Raman scattering measurements of combustion properties, in : Laser Probes for Combustion Chemistry (Ed. by D.R. Crosley), Am. Chem. Soc. Symp. Series, Vol. 134, Washington, D.C., 1980.

[58] - M. Lapp and R.M.C. So, The study of turbulent diffusion flames, Modeling needs and experimental light scattering capabilities, presented at the 55th (A) Specialist's Meeting of the AGARD propulsion and energetics panel, Brussels, Belgium, 5-7 May, 1980.

[59] - S. Lederman and J. Bornstein, Specie concentration and temperature measurements in flowfields project SQUID. Techn. Rep. PIB-31-PU (1973).

[60] - S. Lederman, J. Bornstein, A. Celentano and J. Glaser, Temperature, concentration and velocity measurements in a jet and flame. Project SQUID Techn. Rep. PIB-33-PU (1973).

[61] - S. Lederman, Some applications of laser diagnostics to fluid dynamics, AIAA Paper n° 76-21 (1976).

[62] - W.D. Williams, H.M. Powell, R.L. Mc Guire, L.L. Price, J.H. Jones, D.P. Weaver and J.W.L. Lewis, AIAA Paper n° 77-211 (1977)

[63] - M. Péalat, R. Bailly and J.P.E. Taran, Opt. Commun., 22, 91-94(1977).

[64] - E. Yablonovitch, N. Bloembergen and J.J. Wynne, Phys. Rev., B3, 2060 (1971).

[65] - S.A. Akhamanov, V.G. Dmitriev, A.I. Kovrigin, N.I. Koroteev, V.G. Tunkin and A.I. Kholodnykh JETP Letters, 15, 425 (1972).

[66] - M.D. Levenson, C. Flytzanis and N. Bloembergen, Phys. Rev., 6, B3962 (1972).
N. Bloembergen, Nonlinear optics, W.A. Benjamin Inc. Publishers (1965).

[67] - W.G. Rado, Appl. Phys. Lett., 11, 123 (1967).

[68] - G. Hauchecorne, F. Kerhervé and G. Mayer, J. de Physique, 32, 47 (1971).

[69] - F. De Martini, G.P. Guiliani and E. Santamato, Opt. Commun. 5, 126 (1972).

[70] - P.R. Régnier and J.P.E. Taran, Appl. Phys. Lett., 23, 240 (1973).

[71] - M. Péalat, S. Druet, B. Attal and J.P.E. Taran, Temperature and concentration measurements in reactive media by coherent anti-Stokes Raman scattering, 16th International Symposium on Combustion, Aug. 1977, pp. 789-798.

[72] - M. Péalat, J.P.E. Taran and F. Moya, Optics and Laser Technology, 12, 21 (1980).

[73] - J.W. Nibler, W.M. Shaub, J.R. Mc Donald, and A.B. Harvey, Coherent anti-Stokes Raman spectroscopy, p. 173 in Vibrational spectra and structure, vol. 6, J.R. Durig (Editor), Elsevier, Amsterdam, 1977.

[74] - J.W. Nibler and G.V. Knighten, Coherent anti-Stokes Raman spectroscopy, in topics in current physics, Chap. 7, A. Weber (Editor), Springer Verlag, Berlin, New York, 1977.

[75] - A.C. Eckbreth, R.J. Hall and J.A. Shirley, Investigations of CARS for combustion diagnostics, AIAA 17th Aerospace Sciences Meeting, New-Orleans, La., Jan. 15-17, 1979, AIAA Paper n° 79-83.

[76] - I.R. Beattie, J.D. Black, T.R. Gilson and D.A. Greenhalgh, Coherent anti-Stokes Raman spectroscopy in sooty diffusion flames, SPIE Paper n° 158-09, August 1978.

[77] - J.P.E. Taran, CARS flame diagnostics, presented at the CARS Meeting of the Institute of Physics, AERE Harwell, March 1979.

[78] - B. Attal, M. Péalat and J.P.E. Taran, CARS diagnostics of combustion presented at AIAA, 18th Aerospace Sciences Meeting, Pasadena, California, Jan. 14-16th, 1980, AIAA Paper n° 80-282 ; also J. Energy, 4, 135 (1980).

[79] - G.L. Switzer, W.M. Roquemore, R.B. Bradley, W.P. Schreiber and W.B. Roh, CARS measurements in a bluff-body stabilized diffusion flame, Applied Optics, 18, 2343 (1979).

[80] - A.C. Eckbreth and R.J. Hall, Combustion and flame, 36, 87 (1979).

[81] - J.W. Nibler, J.R. Mc Donald and A.B. Harvey, Opt. Commun., 18, 371 (1976) ;
W.M. Shaub J.W. Nibler and A.B. Harvey, J. Chem. Phys., 67, 1883 (1977).

[82] - M. Péalat, J.P.E. Taran, J. Taillet, M. Bacal and A.M. Bruneteau, J. Appl. Phys., to be published.

[83] - W.B. Roh, P.W. Schreiber and J.P.E. Taran, Applied Physics Letters, 29, 174 (1976).

[84] - A.C. Eckbreth, CARS investigation in flames, Paper presented at the 17th International Symposium on Combustion, Leeds, England, August 1978.

[85] - J.J. Barrett and R.F. Begley, Appl. Phys. Lett., 27, 129 (1975).

[86] - M.A. Henessian, L. Kulevskii and R.L. Byer, J. of Chem. Phys., 65, 5530 (1976).

[87] - A. Hirth and K. Volrath, Opt. Commun., 18, 213 (1976).

[88] - W. Nitsch and W. Kiefer, Opt. Commun., 23, 240 (1977).

[89] - I.R. Beattie, T.R. Gilson and D.A. Greenhalgh, Nature 276, 378 (1978).

[90] - A. Laubereau and W. Kaiser, Rev. Mod. Phys., 50, 607 (1978).

[91] - I. Chabay, G.K. Klauminzer and B.S. Hudson, Appl. Phys. Lett., 28, 27 (1976).

[92] - L.A. Carreira, L.P. Gross and T.B. Malloy, Jr., J. Chem. Phys., 69, 855 (1978).

[93] - B. Attal, O.O. Schnepp and J.P.E. Taran, Opt. Commun., 24, 77 (1978).

[94] - D.M. Guthals, K.P. Gross and J.W. Nibler, J. Chem. Phys., 70, 2393 (1979).

[95] - S.A.J. Druet, J.P.E. Taran and Ch. J. Bordé, J. de Phys., 40, 819 (1979) and ibid., 41, 183 (1980).

[96] - S.A.J. Druet, B. Attal, T.K. Gustafson and J.P.E. Taran, Phys. Rev., A18, 1529 (1978).

[97] - S.A.J. Druet and J.P.E. Taran, Coherent anti-Stokes Raman spectroscopy, in : Chemical and Biochemical Applications of Lasers, vol. 4, edited by C.B. Moore, Academic Press, New York (1979).

[98] - S.Y. Yee, T.K. Gustafson, S.A.J. Druet and J.P.E. Taran, Opt. Commun., 23, 1 (1977).

[99] - J. Bordé and C.H. Bordé, J. Mol. Spectrosc., 78, 3530 (1979).

[100] - A. Omont, E.W. Smith and J. Cooper, The Astroph. J., 175, 185 (1972).

[101] - A.C. Eckbreth, Appl. Phys. Letters, 32, 421 (1978).

[102] - L.A. Rahn, L.J. Zych and P.L. Mattern, Opt. Commun., 30, 249 (1979).

[103] - K.P. Gross, D.M. Guthals and J.W. Nibler, J. Chem. Phys., 70, 4673 (1979).

[104] - M.E. Mc Ilwain and J.C. Hindman, J. Chem. Phys., 73, 68 (1980).

[105] - S.A.J. Druet and J.P.E. Taran, to be published in Progress in Quantum Electronics.

[106] - P. Luc, J. of Mol. Spectros., 80, 41 (1980).

[107] - S. Gerstenkorn and P. Luc, Atlas du spectre d'absorption de la molécule d'iode, Editions du C.N.R.S., Paris, 1978.

Achevé d'imprimer à l'ONERA, septembre 1981 — Dépôt légal 3e trimestre 1981 - n° 636.